The Texas Medical Center Library
DigitalCommons@TMC

Dissertations and Theses (Open Access)

MD Anderson UTHealth Houston Graduate School

8-2022

Yap And Taz Are Required For Neural Crest-Derived Cardiovascular Development

Shannon Erhardt

Follow this and additional works at: https://digitalcommons.library.tmc.edu/utgsbs_dissertations

Part of the Biology Commons, Cell and Developmental Biology Commons, Genetics and Genomics Commons, and the Medical Sciences Commons

Recommended Citation

Erhardt, Shannon, "Yap And Taz Are Required For Neural Crest-Derived Cardiovascular Development" (2022). *Dissertations and Theses (Open Access)*. 1217.
https://digitalcommons.library.tmc.edu/utgsbs_dissertations/1217

This Thesis (MS) is brought to you for free and open access by the MD Anderson UTHealth Houston Graduate School at DigitalCommons@TMC. It has been accepted for inclusion in Dissertations and Theses (Open Access) by an authorized administrator of DigitalCommons@TMC. For more information, please contact digcommons@library.tmc.edu.

Yap and *Taz* are Required for Neural Crest-Derived Cardiovascular Development

by

Shannon Nicole Erhardt, B.S.

APPROVED:

Jun Wang, Ph.D.
Advisory Professor

Richard Behringer, Ph.D.

Peter Lwigale

Peter Lwigale, Ph.D.

James Martin, M.D., Ph.D.

Rachel K. Miller

Rachel Miller, Ph.D.

APPROVED:

Dean, The University of Texas
MD Anderson Cancer Center UTHealth Graduate School of Biomedical Science

Yap and *Taz* are Required for Neural Crest-Derived Cardiovascular Development

A

THESIS

Presented to the Faculty of

The University of Texas

MD Anderson Cancer Center UTHealth

Graduate School of Biomedical Sciences

in Partial Fulfillment

of the Requirements

for the Degree of

MASTER OF SCIENCE

by

Shannon Nicole Erhardt, B.S.
Houston, Texas

August, 2022

Dedication

I dedicate this thesis to my family, who have pushed me to be the best version of myself in all aspects of my life.

Acknowledgements

I would first like to thank my advisor, Dr. Jun Wang, for being a great mentor and providing an enormous amount of support throughout my master's degree. She has been extremely supportive of my future endeavors and has pushed me to be the best version of myself both in and out of the laboratory. She has provided valuable insight from her own experiences, allowing my critical thinking, organizational, and technical skills to massively advance. Furthermore, she has encouraged me to step out of my comfort zone regarding scientific presentations and scientific writing, for which I am extremely grateful. I know I would not have been able to accomplish what I have in these past two years without her. I greatly appreciate all the current and past members of the Wang laboratory. I want to thank Dr. Xiaolei (Sherry) Zhao for her willingness to assist me with any minor details regarding experimental planning and analysis. I would also like to thank Wen (Grace) Chen, who welcomed me to lab every day with a smile and dedicated her time to ensure I developed strong and proper mouse-handling techniques. To Tram Le and Shaungjie You, thank you for your constant advice and help regarding cell and sequencing data for my project, and for allowing me to share my personal experiences and endeavors with you. I would like to give a special thank you to Dr. Mingjie Zheng for being an amazing bench mentor. He has dedicated an immense number of hours to helping me become a better, well-rounded, scientist. From the beginning, he has always been extremely patient with me and dedicated his time to ensure I am not only able to get results but that I have an extended understanding of the purpose of each experiment. I know you will become a wonderful PI in the near future.

Furthermore, I would like to thank my advisory committee members (Drs. Richard Behringer, Peter Lwigale, James Martin, and Rachel Miller). Although we were only able to

hold a few meetings during my time as a student, each member was incredibly supportive, provided valuable suggestions, and proposed in-depth questions that made me think more critically about experimental details and designs.

I want to thank the Genetics and Epigenetics program for being an amazingly social and supportive group. The faculty always showed personal interest and excitement in each student's work, which has established numerous personal and academic connections. To all the students, thank you for being such as welcoming and friendly group, despite not being able to meet in person during most of my time due to the COVID-19 pandemic. I want to give a huge thank you to Elisabeth Lindheim who welcomed me with open arms and was there for me in both good and bad times. She provided me with endless support, pushing me to become a well-rounded student. Thank you to the deans and administrators for not only providing an exceedingly supportive environment but also ensuring that the needs of students were always at the forefront.

I am immeasurably grateful to my friends who were always willing to listen about my scientific endeavors while also allowing me to take a mental break from science. I want to thank my boyfriend, Justin Moore, who has been incredibly supportive of my ambitious undertakings and has always believed I would go on to accomplish all I set my mind to. Lastly, I would like to thank my family. To my sister, Molly, you have never given up during your time as a student which has only pushed me to give my very best. To my mother, you are my biggest supporter and have always believed in me even when I had given up on myself. I could not have gotten here today without your support. I love you both.

Yap and _Taz_ are Required for Neural Crest-Derived Cardiovascular Development

Shannon Nicole Erhardt, B.S.

Advisory Professor: Jun Wang, Ph.D.

Congenital heart defects (CHDs) are the most common human birth defect, occurring in ~1/100 newborns, and are a leading cause of early infant death. Cardiac neural crest cells (NCCs) are a migratory and multipotent cell population known to aid in the development of the cardiac outflow tract (OFT), valves, and interventricular septum, during embryogenesis. *Yap* and *Taz* are downstream effectors of the fundamental Hippo signaling pathway and are vital for proper organ and tissue development, yet their role in neural crest (NC)-derived heart formation is still largely unknown. We generated *Yap* and *Taz* conditional knockout (CKO) mice using a Cre-lox system, by the use of *Yap* and *Taz* CKO alleles and the NC-specific Cre drivers *Wnt1-Cre* and *Wnt1-Cre2SOR*, which leads to abnormal cardiac formation, mimicking human CHD phenotypes. $Yap^{+/-}; Taz^{-/-}$ CKO mutants produced various OFT and remodeling defects including ventricular septal defect (VSD), tetralogy of Fallot (TOF), double outlet right ventricle (DORV), and cardiac valve aberrations, varyingly between embryonic day (E) 14.5, E16.5, and E18.5. Cell apoptosis, proliferation, and smooth muscle differentiation were unchanged in $Yap^{+/-}; Taz^{-/-}$ CKO mutants. Comparably, $Yap^{+/-}; Taz^{+/-}$ double heterozygous hearts exhibited external morphology similar to that of controls, but sectioning revealed mild VSD, along with cardiac valve leaflet irregularities, at E16.5 and E18.5. Compelling preliminary RNA-sequencing data together with transwell migration assay, scratch assay, and *ex vivo* culture, indicate a potential role for *Yap/Taz* in regulating NC migration. Together, our data indicate that *Yap/Taz* play a critical role in proper cardiac NC-derived cardiac formation.

Table of Contents

Approval Page…….....i

Title Page…..……..ii

Dedication……..iii

Acknowledgements……..……..iv

Abstract……..……vi

Table of Contents…….……..…vii

List of Figures……ix

List of Tables……..……..…..xi

List of Abbreviations……...……..xii

Chapter 1:Introduction……1

1.1 Heart Anatomy and Function...……1

1.2 Heart Development.……..... ……...……3

1.3 Neural Crest Cells……4

1.4 Cardiac Neural Crest Cells...……...……5

1.5 Hippo-YAP Signaling Pathway.……... ……..6

1.6 Hippo-YAP Signaling in Heart Development…….9

1.7 Neural Crest Contribution to Disease..…….…… …….11

1.8 Congenital Heart Defect……...……..12

1.9 Regulation of Neural Crest-Derived Congenital Heart Defects……..……...13

Chapter 2: Statement of Objectives……...……17

2.1 Knowledge Gap……..……...……..17

2.2 Hypothesis……...……...17

2.3 Aims and Experimental Approach…….……18

Chapter 3:
Methods…….……...…….19

3.1 Generation of Transgenic Mouse Line…….…….…….19

3.2 Histology and Hematoxylin and Eosin Staining……19

3.3 EdU Staining and Immunohistochemistry…….……20

3.4 Genotyping of Embryos…….……21

3.5 TUNEL Assay……21
3.6 O9-1 Cell Culture and siRNA Knockdown for Transwell Migration and Scratch Assay..22
3.7 *ex vivo* OFT Explant Culture……..……...……23
3.8 RNA Extraction for Ultra-low Bulk RNA-sequencing……..……24
3.9 Cell Counts and Statistical Analyses..……..……..……25
Chapter 4: Results……...……..26
4.1 *Yap/Taz* Combinational Deficiencies in Neural Crest Cells Alters Cardiac Structure…...26
4.2 *Yap/Taz* Combinational Deficiencies in Neural Crest Cells Alters Cardiac Anatomy…...35
4.3 Investigation into the Role of *Yap* and *Taz* in Neural Crest Cell Fate During Cardiac Development..……..44
4.4 *Yap/Taz* Deficiencies in the Neural Crest Impair Cell Migration……..51
4.5 RNA-sequencing Reveals a Role for the Hippo-Yap Pathway in Neural Crest Migration…….....…55
Chapter 5: Discussion, Future Directions, and Conclusions…….……..……..58
5.1 Discussion.……58
5.2 Future Directions……...61
5.3 Conclusions…….……..……63
Chapter 6: Bibliography……..…….64
Vita……..……..79

List of Figures

Figure 1: The Mammalian Heart……..2

Figure 2: The Canonical Hippo Signaling Pathway in Mammals……8

Figure 3: Congenital Heart Defects Associated with Neural Crest Deficiencies……16

Figure 4: *Yap/Taz* mutant embryos display disrupted cardiac morphology at E18.5…….30

Figure 5: Main vessel defects in mutant embryos at E16.5……..…30

Figure 6: E14.5 mutant hearts do not have structural defects…….30

Figure 7: Cardiac outflow tract morphology is unchanged in mutant and double homozygous embryos at E10.5…….31

Figure 8: Cardiac outflow tract structure is unchanged in mutant embryos at E9.5…….…..32

Figure 9: Double heterozygous embryos present with minor cardiac anatomy defects at E18.5……....33

Figure 10: E16.5 double heterozygous embryos have minor main vessel mispositioning….33

Figure 11: E14.5 double heterozygous embryos have no variation in cardiac structure……33

Figure 12: Outflow tracts of double heterozygous embryos at E10.5 have no structural defects……..34

Figure 13: Sectioning reveals altered cardiac morphology in mutant embryos at E18.5……37

Figure 14: Various cardiac defects in mutant embryos at E16.5……...…….38

Figure 15: Ventricular septal defect is evident in mutant embryos at E14.5……...…...39

Figure 16: E18.5 double heterozygous hearts present with ventricular septal defect and double outlet right ventricle…….41

Figure 17: Sectioning reveals ventricular septal defect in double heterozygous hearts at E16.5……42

Figure 18: No cardiac defects in double heterozygous hearts at E14.5……....43

Figure 19 Proliferation rates are unchanged in the cardiac outflow tract of E9.5 mutant embryos……...……..…46

Figure 20: Proliferation rates are unchanged in the cardiac outflow tract of E10.5 mutant embryos……47

Figure 21: Smooth muscle differentiation is unchanged in the cardiac outflow tract of E9.5 mutant embryos……48

Figure 22: E10.5 mutant samples do not display altered smooth muscle differentiation in the cardiac outflow tract……..……...49

Figure 23: Apoptosis is unchanged in the outflow tract of E9.5 mutant samples……..50

Figure 24: *ex vivo* migration assay of the cardiac outflow tract from double heterozygous embryos at E10.5 displays inhibited migration……...…….53

Figure 25: Inhibited O9-1 neural crest cell migration with deficiencies of *Yap* and *Taz*…...54

Figure 26: Inhibited migratory abilities of O9-1 cells with deficiencies of *Yap* and *Taz*…...55

Figure 27: GO term analysis reveals downregulated terms from Ultra-low Bulk RNA-sequencing…….……...56

Figure 28: Downregulation of cell migration and ECM organization genes …….57

List of Tables

Table 1: Total number of embryos using *Wnt1-Cre*……..….29

Table 2: Total number of embryos using *Wnt1-Cre2SOR*……..29

Table 3: Cardiac phenotypic rates of *Yap* and *Taz* alterations using *Wnt1-Cre* at different developmental stages……...36

Table 4: Cardiac phenotypic rates of *Yap* and *Taz* alterations using *Wnt1-Cre2SOR* at different developmental stages……...36

List of Abbreviations

aSMA: mouse-anti-actin, α-Smooth Muscle-Cyan3

Bmpr1a: Bmp receptor 1A

Bmps: bone morphogenetic proteins

CHDs: congenital heart defects

CDH7: chromodomain helicase DNA binding protein 7

DAPI: 4',6-Diamidino-2-Phenylindole, Dihydrochloride

DORV: double outlet right ventricle

ECM: extracellular matrix

EdU: 5-ethynyl-2'-deoxyiridine

EMT: epithelial-to-mesenchymal transition

FBS: fetal bovine serum

FHF: first heart field

Foxc1/2: forkhead box C1/C2

FPKM: fragments per kilobase million

GO: gene ontology

Hand2: heart and neural crest derivatives expressed 2

H&E: hematoxylin and eosin

IHC: immunohistochemistry

IVS: intraventricular septum

Jag1: jagged 1

Lats1/2: large tumor suppressor homologue 1 and 2

MST1/2: mammalian sterile 20-like protein kinase 1 and 2

NC: neural crest

NCCs: neural crest cells

OFT: outflow tract

PBS: phosphate-buffered saline

PTA: persistent truncus arteriosus

RNA-seq: RNA-sequencing

SAV1: salvador homologue 1

SHF: second heart field

Taz: transcriptional coactivator with PDZ-binding motif

TEADs: TEA domain transcription factor family members

TOF: tetralogy of fallot

VSD: ventricular septal defect

Yap: Yes-associated protein

Chapter 1: Introduction

1.1 Heart Anatomy and Function

The heart is a muscular organ that functions in pumping blood to continuously supply oxygen and other nutrients throughout the body. The heart is further responsible for maintaining heart rate and controlling blood pressure.

Anatomically, the heart is a complex, multi-layered organ. In mammals, the walls of the heart consist of three layers (epicardium, myocardium, and endocardium) enclosed in the pericardium, a membrane-like sac that surrounds the heart [1] (Figure 1). The epicardium is the outermost layer, followed by the middle layer deemed the myocardium, and the endocardium, the innermost layer. The heart is divided into right and left halves, and further subdivided into the upper and lower cavities, separating the heart into four chambers: right atrium, left atrium, right ventricle, and left ventricle (Figure 1). The heart also consists of a variety of vessels, that carry blood to the heart, along with arteries, that carry blood away from the heart. Furthermore, the heart consists of what is known as the great or main vessels, which are the major arteries and veins that carry blood. The main two vessels connected directly to the heart are the aorta and the pulmonary vessel [2].

The complexity of the heart means that this organ is also very specific in the way it functions and the way blood flows. Venus, or deoxygenated, blood from the body enters the right atrium, via the vena cava, a large vein that carries blood to the heart. The right atrium then pumps this blood into the right ventricle, through the tricuspid valve. The right ventricle then pumps the blood through the semilunar valve, into the pulmonary trunk to reach the lungs, where oxygenation of the blood occurs.

After being oxygenated in the lungs, blood enters the left atrium via the pulmonary veins. The left atrium pumps blood through the mitral valve into the left ventricle, which then pumps this blood through the semilunar valve of the aorta to supply the body with oxygenated blood (Figure 1).

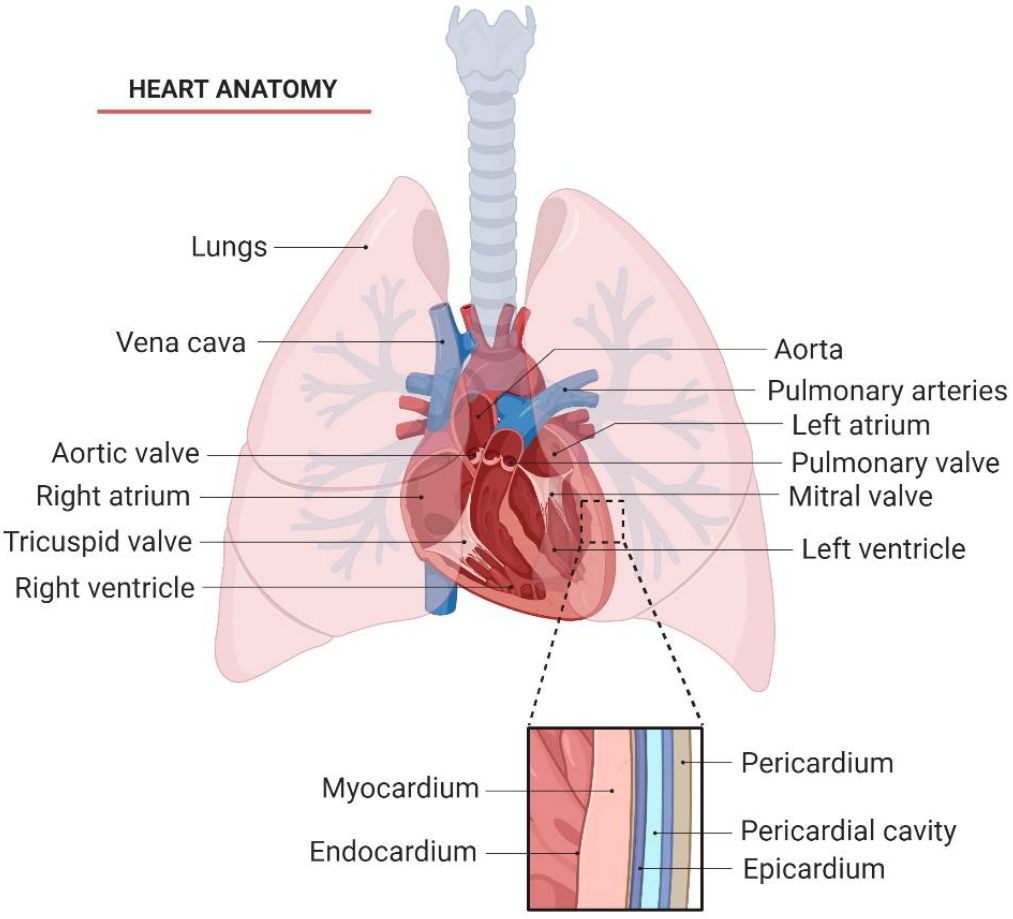

Figure 1: The Mammalian Heart

The heart functions to provide oxygenated blood, along with various nutrients, to the body. There are three layers to the walls of the heart: the epicardium, myocardium, and endocardium. The heart is comprised of four chambers, separated both vertically and horizontally: right atrium, left atrium, right ventricle, and left ventricle, along with numerous veins and arteries, including the aorta and the pulmonary vessel. The heart functions by taking de-oxygenated blood from the body, transporting the blood to the lungs where oxygenation occurs, and then pumping this oxygenated blood to the body. Created with BioRender.

1.2 Heart Development

In humans, the heart is one of the first organs to form and function. Around gestational week 2, cardiac tissue is organized into what is referred to as the ‘cardiac crescent’ consisting of cells from pre-cardiac mesodermal cells [3]. Mesodermal cells that are differentiating into cardiomyocytes begin to become electrically competent. Around week 3 of gestation the linear heart tube, which maintains contractile beats and continuous blood flow, begins to form but does not contain a distinguishable cardiac conduction system [4]. Nearing the end of gestational week 3, the fetal heart becomes vital for oxygen and nutrient distribution. By gestational week 4, the heart tube undergoes looping to provide proper positioning to form the four chambers of the heart. Due to the continuous addition of new cardiomyocytes, derived from mesodermal cells, the looping heart continues to grow [5]. Upon looping, ventricle formation begins to take place and the cardiac jelly, located between the endocardial and myocardial layers, disappears and trabeculations become evident [5]. During ventricular development, the atria begin to form with specific left-right identity. Heart septation is a complex process that when disrupted, may result in cardiac congenital abnormalities and death. During this fourth week of development, the ventricular septum begins to lengthen. From the fifth week of development and further, the outflow tract (OFT), a myocardial tube that runs from the developing ventricles to the aortic sac, becomes shorter, contributing to a portion of the ventricular septum, along with portions of the aortic and pulmonary trunks [6].

The heart is derived from a variety of multipotent progenitor cells including those of the first heart field (FHF), second heart field (SHF), and neural crest cells

(NCCs) [5,6]. Cells of the FHF mainly populate the ventricles and atria, whereas progenitor cells from the SHF will give rise to the myocardium, endothelial cells, and smooth muscle of the heart [5,6]. NCCs that travel to the heart will assist in the development of the cardiac OFT, aorta and pulmonary trunks, and a portion of the septum [4,6].

1.3 Neural Crest Cells

The neural crest (NC) is a multipotent and migratory embryonic cell population necessary during vertebrate development. NCCs originate in the dorsal-most region of the neural tube [7-9]. Upon the closure of the neural plate and the subsequent formation of the neural tube, a process known as neurulation, cells that remain a part of the neural tube assist in forming the brain and spinal cord, while cells that were part of the neural plate begin to delaminate and are referred to as NCCs. Simultaneously, NCCs obtain their migratory potentials from a process known as epithelial-to-mesenchymal transition (EMT) [10]. EMT is a necessary step in the proper formation and contribution of NCCs to embryogenesis [10-12]. Once NCCs are released from the neural tube, they migrate throughout the embryo dependent on both their initial axial level position and terminal sites for differentiation. NCCs have the ability to differentiate into a wide variety of cell derivatives, including smooth muscle cells, osteoblasts, pigment cells, and neurons [13,14]. It is generally assumed that there are four main subpopulations of NCCs: cranial, trunk, vagal, and sacral. However, further investigation into such subpopulations has indicated that the vagal NC consists of a smaller specified subpopulation deemed the cardiac NC [9,15,16]. The investigation

into such subpopulations has expanded the regulatory capacity of the NC, leading to the identification of various functions and contributing processes.

1.4 Cardiac Neural Crest Cells

The cardiac NC is a specific subpopulation of the vagal NC [9,16]. Cardiac NCCs are known to significantly contribute to cardiovascular development, along with aiding in the development of the thymus, thyroid glands, and cardiac ganglia. NC ablation studies have demonstrated the necessity of NCCs for proper heart formation [9,17-19]. In the mammalian and chick heart, cardiac NCCs contribute greatly to the patterning and septation of the OFT and pharyngeal arch arteries, contributing to the aorta and pulmonary valves [20-22]. Cardiac NCCs also contribute to the upper-most portion of the interventricular septum (IVS) and the parasympathetic innervation of the heart [20,21]. Cardiac NC-derived cells contribute to the vascular smooth muscle of the aorta, pulmonary artery, ductus arteriosus, and a portion of the carotid [23]. It is important to note that although NCCs are necessary for vertebrate embryogenesis, cardiac NCC function differs between vertebrates [9]. It was found that in both mammals and chicks, the cardiac NC has similar migration and contribution patterns; however, these vertebrates show varying contributions regarding the timing of NC contribution to OFT development [19,24]. In contrast to the functions in amniotes, cardiac NCC contribution varies in zebrafish and *Xenopus laevis*, simply due to their cardiac structural differences. The zebrafish heart is comprised of a single atrium and ventricle, along with a single-loop circulatory system that does not require OFT septation. Furthermore, cardiac NCCs have been shown to potentially contribute to cardiomyocytes in zebrafish, while this is still unclear in amniotes [25,26]. Similar to

zebrafish, the hearts of *Xenopus laevis* are comprised of a single ventricle with three distinct chambers, along with having incomplete septation of the OFT, a structure shown to not be contributed by cardiac NCCs in this model [27,28]. Yet, cardiac NCCs in *Xenopus laevis* do contribute to the aortic arch and aortic sac, as seen in amniotes [28,29]. Although cardiac NC contribution varies between species, there is no doubt about the importance of their contribution to proper embryonic development.

1.5 Hippo-YAP Signaling Pathway

The Hippo-YAP (Yes-associated protein) signaling pathway, initially discovered in *Drosophila melanogaster*, is a highly conserved pathway necessary for the regulation of organ size and development [30-32]. The Hippo signaling pathway is a known kinase cascade, consisting of highly conserved elements, that has been indicated in embryonic organogenesis and cell fate determination. In mammals, the first components of this pathway are protein salvador homolog 1 (SAV1) and mammalian sterile 20-like protein kinase 1 and 2 (MST1/2), followed by the large tumor suppressor homolog 1 and 2 (Lats1/2) and the scaffolding protein MOB (Figure 2). The activation of this pathway relies on the upstream phosphorylation of the SAV1-MST1/2 kinase complex. This pathway can be regulated by a variety of factors such as micro-RNAs, mechanical signaling, and physiological regulators such as cell-adhesion molecules and cell polarity [33,34]. When Hippo signaling is active, the SAV1-MST1/2 complex is phosphorylated and in turn, phosphorylates the LATS1/2-MOB complex. The primary targets of this kinase cascade are the downstream co-activators YAP and TAZ (transcriptional coactivator with PDZ-binding motif). Phosphorylated LATS1/2-MOB then phosphorylates the YAP/TAZ complex. The phosphorylation-

repressive activity of this pathway inhibits transcription and promotes retention and degradation of YAP/TAZ in the cytoplasm (Figure 2). However, without the repression of the Hippo-Yap signaling pathway, YAP/TAZ are not phosphorylated and can translocate to the nucleus (Figure 2). Due to YAP/TAZ not having a DNA-binding domain, the YAP/TAZ complex is dependent on transcription factors, such as the TEA domain transcription factor family members (TEADs), to create a large complex allowing for the transcription of target genes, usually associated with cell fate.

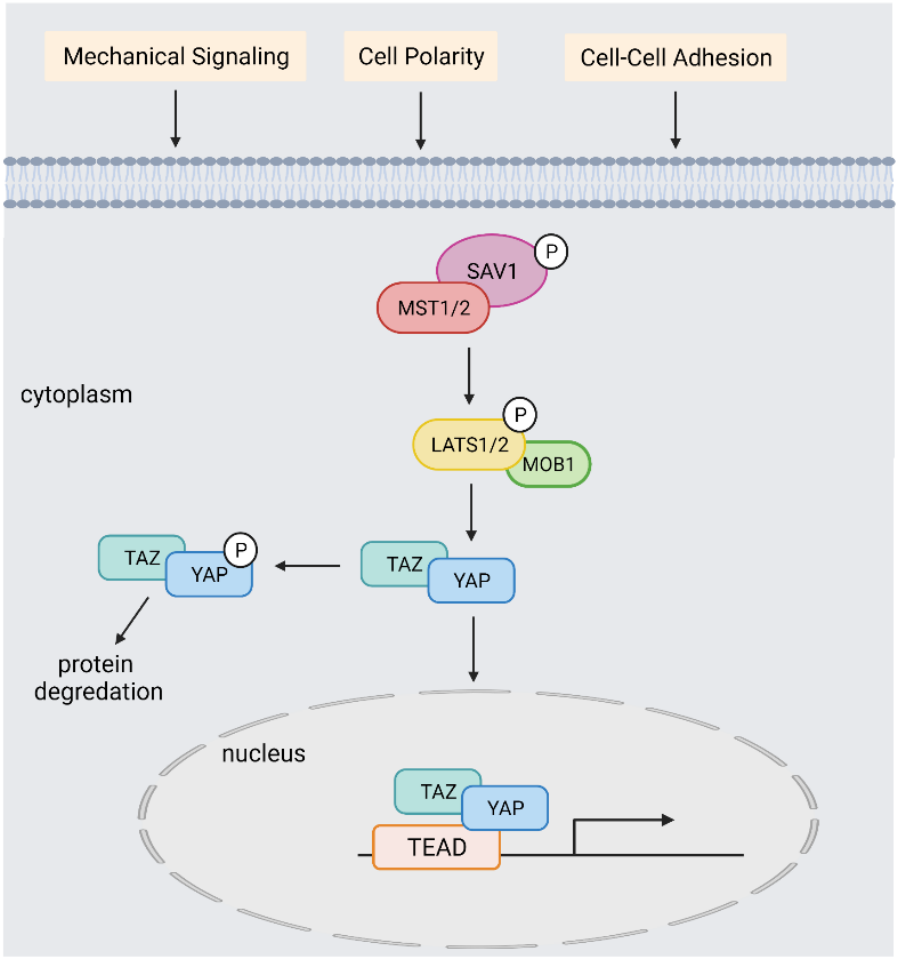

Figure 2. The Canonical Hippo Signaling Pathway in Mammals

The mammalian Hippo signaling pathway is a negative-regulatory pathway necessary for the development of a variety of organs and tissues. The most upstream components, SAV1 (protein salvador homolog 1)-MST1/2 (mammalian sterile 20-like protein kinase 1 and 2), can become phosphorylated due to various external factors including mechanical signaling, cell fate, and cell-cell adhesion. Phosphorylated SAV1-MST1/2 then phosphorylate LATS1/2 (large tumor suppressor homolog 1/2) and MOB. Once LATS1/2-MOB is phosphorylated, they phosphorylate the downstream co-effectors YAP (Yes-associated protein) and TAZ (transcriptional co-activator with PDZ binding motif). Once phosphorylated, YAP/TAZ are retained in the cytoplasm, where protein degradation occurs. When the Hippo pathway is off or inactive, phosphorylation of the kinase cascade does not occur, allowing non-phosphorylated YAP/TAZ to translocate into the nucleus and interact with transcription factors such as TEAD (TEA domain transcription factor family members), to regulate cell fate. Created with BioRender.

1.6 Hippo-YAP Signaling in Heart Development

The Hippo-YAP signaling pathway is vital for proper organ and tissue development, with roles in cell fate. In regards to heart development, the Hippo-Yap pathway is essential for maintaining proper heart size, while deficiencies or inhibitions result in severe cardiac defects and lethality.

Hippo signaling is expressed in cells of the three cardiac layers: myocardium, epicardium, and endocardium. It was found that the individual cardiac-specific deletion of the core Hippo components *Sav1, Mst1/2,* and *Lats2,* by use of $Nkx2.5^{Cre}$, resulted in expanded trabecular and subcompact ventricular myocardial layers [35]. Furthermore, hearts with the complete deletion of *Sav1* presented with overall heart enlargement made evident by large ventricular chambers, which did not distill from an alteration of myocardial cell size [35]. Regarding the epicardium, conditional deletion of *Lats1* and *Lats2*, by use of $Wt1^{CreERT2}$, led to embryonic lethality by embryonic day (E) 15.5 presenting with an overall smaller heart, less compact myocardium, and vasculature defects [36]. Interestingly, embryos with the epicardium-specific deletion of both *Lats1* and *Lats2,* with heterozygous deletions of the Hippo downstream effectors *Yap* and *Taz* were viable and did not display vascular defects, while epicardial inactivation of only *Yap* and *Taz* led to embryonic lethality between E11.5 and E12.5, with altered coronary vascular development in the heart [36,37]. Postnatal lethality was observed in mice with the deletion of both *Yap* and *Taz* in endocardial cells, by use of the $Nfatc1^{IRES\text{-}Cre/+}$ allele, along with ventricular septation defects and thinner myocardium of the ventricular walls as compared to controls [38].

Besides the role of the Hippo pathway in specific structural components of the heart during development, investigations have been made into the role of this pathway in cardiac progenitor populations. As previously established, during early cardiac development, the mammalian heart is referred to as the cardiac crescent, being comprised of two precursor cell populations; the FHF and SHF. Cells of the FHF initially contribute to the linear heart tube and cardiac jelly and later assist in the formation of the left ventricle [5,39,40]. SHF progenitors will assist in the formation of the outflow tract, right ventricle, and atria [5,40]. Both the FHF and SHF contribute to the populations of cardiomyocytes in the heart. The function of the Hippo-Yap pathway in cardiomyocytes has been investigated previously. Deletion of *Mst1/2* promoted cardiomyocyte proliferation during cardiac development [35]. Similar findings displayed that constitutively active Yap, in the embryonic heart, increased cardiomyocyte proliferation and heart size, while on the other hand, cardiac deletion of *Yap* reduced cardiomyocyte proliferation [41,42]. In zebrafish, it was found that the restriction of *Yap* and *Taz* to the nucleus caused a lack of cardiac precursor migration to the midline during heart tube formation, resulting in cardia bifida [43].

Besides FHF and SHF precursors another population that contributes heavily to cardiac development is the NC, and more specifically the cardiac NCCs [16,17]. It was initially reported that the complete deletion of the Hippo downstream effectors *Yap* and *Taz* in the NC resulted in embryonic lethality by E10.5, along with branchial arch vasculature defects [9,44,45]. However, the complete deletion of *Yap/Taz* in the NC did not seem to disrupt NC migration at E10.5, particularly to the first arch artery and cardiac OFT, despite the potential role for *Yap* in the regulation of NC progenitors and

cell migration in cancer [45-48]. In the third aortic arch artery, smooth muscle differentiation of NCCs was significantly reduced in embryos with the complete deletion of *Yap/Taz* [45]. However, the role of the Hippo-Yap pathway has yet to be determined regarding cardiac structural formation.

1.7 Neural Crest Contribution to Disease

Deficiencies in NCCs result and contribute to a variety of diseases, including those of the head, nervous system, and heart. Neurocristopathies are a group of diseases and syndromes caused by abnormal development, differentiation, or migration of NCCs during embryogenesis [49]. Syndromes originating from deficiencies in the cranial NC population consist of Craniosynostosis (premature fusion of the cranial sutures), Treacher collins syndrome (hypoplasia of the mandible and a zygomatic complex), and those encompassing cleft lip or palate (openings of the upper lip or roof of the mouth) [49-51]. Alterations in cells of the sacral NC have been shown to contribute to diseases, such as Hirschsprung disease and Waardenburg syndrome type IV, in which patients have an absence of enteric neurons or neural ganglia, respectively [51,52]. Associated diseases regarding alterations to the trunk NC include familial dysautonomia which is caused by a failure in sensory neurogenesis and multiple neuroendocrine tumor-based diseases such as Neuroblastoma and Pheochromocytomas [49,53,54]. Neurocristopathies originating from alterations of the cardiac NC include 22q11.2 deletion syndrome, CHARGE syndrome, and Treacher collins syndrome, all of which present with varying heart defects causing alterations in cardiac structure and function [9,49]. Cardiac defects associated with neurocristopathies can range in type and severity between disorders and patients. Heart malformations during embryo

development, specifically associated with NC deficiencies, are referred to as congenital heart defects (CHDs). Having a basic understanding of NC development and how variations result in such defects, will provide vital information toward disease understanding and treatment.

1.8 Congenital Heart Defect

CHD is a diagnosis given to individuals who have a problem with the structure and/or function of their heart. CHD is present at birth, but may not be diagnosed or recognized until later in one's life. There are a variety of types of CHDs that, depending on the severity, can cause mild or no symptoms, or can disrupt blood flow leading to poor blood circulation and death [9,55,56]. Many children with CHD do not need treatment as their defect is considered mild. However, others whose defects are more severe may need treatment such as medicines, surgeries, or heart transplants. In the United States alone, every one-in-one-hundred newborns are born with CHD, and about one in four babies born with defects have a severe type, needing surgery or another procedure to sustain life [56-58]. To date, there are over ten classified types of CHD, which are categorized by the area of the heart they affect. Most types of CHD affect the walls of the heart, such as the most common defects seen in human cases, Atrial Septal Defect and Ventricular Septal Defect (VSD) (Figure 3) [59-61]. Other common CHDs affect the cardiac OFT, leading to improper development of the aorta and pulmonary vessel, commonly resulting in CHDs such as aortic stenosis and patent ductus arteriosus, and on occasion rarer CHDs such as double outlet right ventricle (DORV) and persistent truncus arteriosus (PTA) (Figure 3) [62-65]. Not only are CHDs categorized as their own disease, but they can also be associated with other defects,

such as in the diseases CHARGE, Treacher Collins, and 22q11.2 deletion syndrome [9,49,66]. Further understanding of how such cardiac defects arise will not only enhance cardiac function and development but will provide a more in-depth understanding of disease treatment.

1.9 Regulation of Neural Crest-Derived Congenital Heart Defects

The regulation of the NC is a long-standing area of investigation. Emphasis has been put on deciphering the molecular regulators that are deficient in NC-derived CHDs to better understand heart development and provide insight into possible treatment options. One component that has provided valuable insight into CHDs is the signaling of bone morphogenetic proteins (Bmps). Bmps are affiliated with the transforming growth factor-beta (TGF-β) family, and are vital for NC induction, migration, and differentiation, with evidence indicating a possible role in cardiac development [9,67-71]. By use of the NC-specific *Wnt1-Cre,* ablation of the Bmp receptor 1A (*Bmpr1a)* in the NC produced shorter cardiac OFTs present with PTA, along with resulting in hypoplastic aortic arch and embryonic lethality (Figure 3) [9,72]. Smad4, a transcription factor located downstream of Bmps and another component of the TGF-β complex, also results in a shortened OFT with PTA, when deleted from NCCs using *Wnt1-Cre* (Figure 3) [9,73]. Furthermore, a recent study of clinical reports regarding children presenting with Myhre syndrome, a rare connective tissue disorder, and tetralogy of Fallot (TOF), poses the hypothesis that Smad4 is a key regulator of NC-derived cardiac development [74]. Another key regulator of cardiac development is the basic helix-loop-helix transcription factor Hand2 (heart and neural crest derivatives expressed 2) [75,76]. *Hand2* conditional knockout in the NC resulted

in hearts with DORV and VSD (Figure 3) [9,77]. Compound NC-specific ablation of Foxc1 and Foxc2 (forkhead box C1/C2), known to be expressed in the NC and NC-derived structures, resulted in a lack of aorticopulmonary septation (PTA) and VSD, while the single NC-specific deletion of *Foxc1* displayed VSD and the single NC-specific deletion of *Foxc2* did not result in obvious abnormalities (Figure 3) [78]. Furthermore, hearts with a double heterozygous deficiency of *Foxc1/2,* in the NC, present with DORV and VSD (Figure 3) [78].

Another highly conserved signaling pathway necessary for the regulation of cell fate, and has shown promising roles in cardiac development is Notch. A number of patients with deletions of the Notch ligand *Jag1* (Jagged 1) presented with TOF and/or stenosis of the pulmonary arteries (Figure 3) [9,79]. Similarly, the inactivation of *Notch2* in the NC, by use of *Pax3-Cre,* resulted in narrowed cardiac OFT arteries [9,80].

Besides certain signaling pathways, there are key transcription factors known to be vital for proper NC-derived cardiac development. Chd7 (chromodomain helicase DNA binding protein 7) is vital for cardiac formation, as its deficiency in NCCs resulted in perinatal lethality with DORV and VSD (Figure 3) [81]. Deletion of *Pitx2,* known to be expressed in the cardiac NC population, results in various cardiac OFT defects such as PTA, DORV, and transposition of the great arteries (Figure 3) [9,82]. Similarly, Tbx1, a well-known gene previously established with 22q11.2 deletion syndrome and known to be expressed by NCCs, is associated with VSD and TOF in patients (Figure 3) [9,83,84]. Furthermore, Tbx1 has been shown to drive NC

migration, and its disruption results in abnormal pharyngeal arch development and aortic interruption [9,85].

Although many signaling pathways and regulators have been shown vital for proper NC-derived cardiac development, investigations are still needed regarding the role and contribution of other signals. Current studies are also working to understand, by using patient-derived data, how such genetic components are altered and uncover the crosstalk between various regulators.

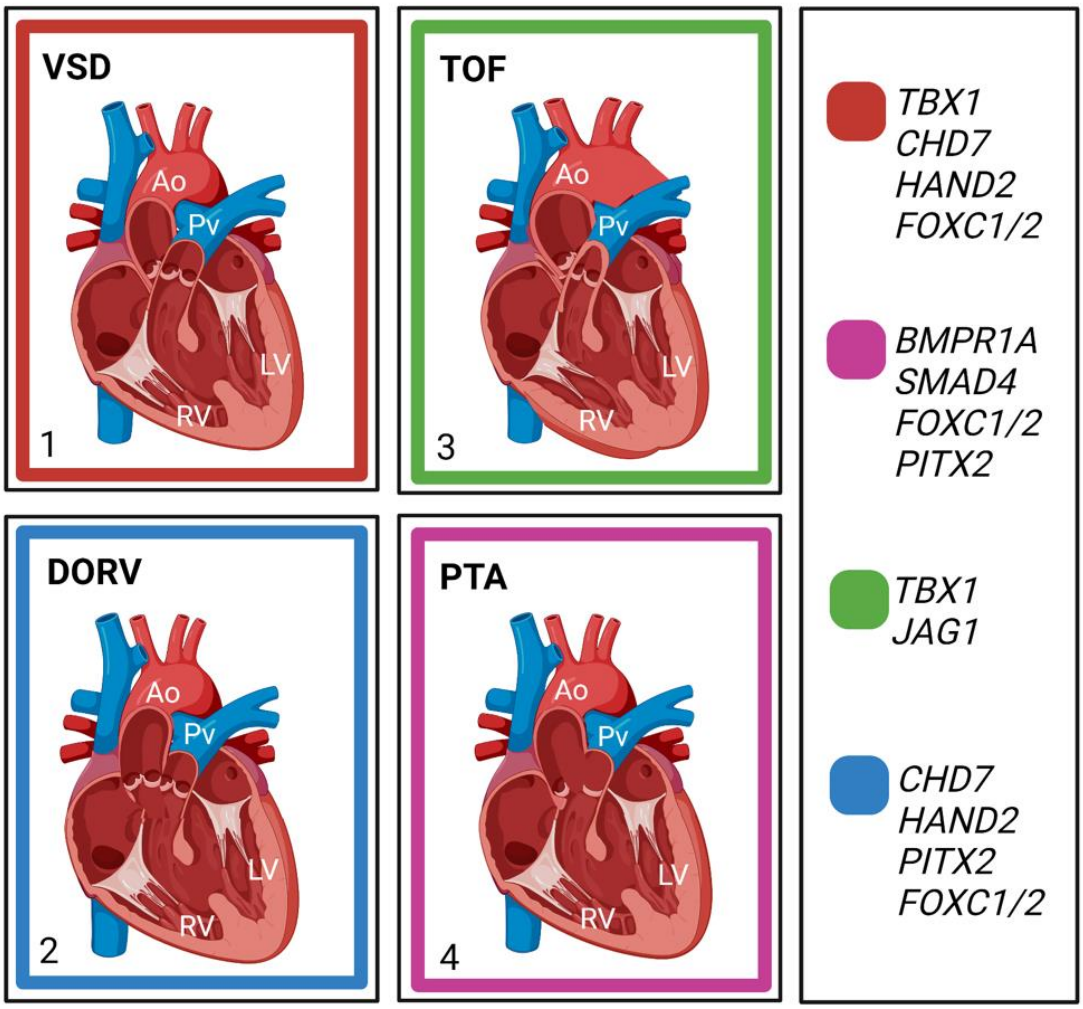

Figure 3. Congenital Heart Defects Associated with Neural Crest Deficiencies

Congenital heart defects resulting from disruption in NC function are depicted in colored boxes. The colors correspond to the genes whose loss or insufficiency in NCCs results in the given phenotype. (1) Red represents ventricular septal defect (VSD) where there is a hole along the interventricular septum. (2) Blue represents double outlet right ventricle (DORV) where both the aorta and pulmonary roots are connected to the right ventricle. DORV phenotype also consists of VSD. (3) Green represents tetralogy of Fallot (TOF) which is characterized by four malformations: VSD, aortic mispositioning, thickened right ventricular wall, and pulmonary stenosis. (4) Magenta represents persistent truncus arteriosus (PTA), where the aorta and pulmonary vessel are not properly separated. PTA also consists of VSD. Created with BioRender.

Chapter 2: Statement of Objectives

2.1 Knowledge Gap

Congenital anomalies of the heart account for over 40,000 live-birth cases of pediatric congenital disease yearly. Although important advances have been made in basic cardiac development research, there are still missing pieces underlying the molecular basis of heart embryogenesis. Being able to uncover vital contributions of signals involved in heart formation will provide a better understanding of development and disease onset as a whole. Previous studies have indicated many causal genes, including those of the Hippo signaling pathways, such as *Yap* and *Taz,* in development. Deficiencies of *Yap/Taz,* particularly in the NC population, a multipotent population noted to be vital for embryogenesis, have shown to be vital for embryonic survival and craniofacial formation, as their deficiencies result in structural defects and death. However, the contribution of *Yap/Taz*, particularly in the NC, to cardiac development is currently limited. Therefore, it is imperative to investigate their contribution through this cell population. This investigation is pivotal for a deeper understanding of cardiac development, while simultaneously providing novel insight into the effects their deficiencies have on heart formation and associated diseases. This rationale formulated the following hypothesis.

2.2 Hypothesis

The Hippo signaling effectors Yap and Taz are required for proper NC-derived heart development.

2.3 Aims and Experimental Approach

Aim 1: Assess cardiovascular formation of embryos with conditional deficiencies of *Yap* and *Taz* in the NC.

Experimental Approach:

- Collect embryos during various in-utero development stages and determine cardiovascular structural alterations.
- Section embryos and embryonic hearts at various stages. Compare the internal structural development between control and *Yap/Taz* deficient samples.

Aim 2: Investigate the function of *Yap* and *Taz* in neural crest cells during cardiovascular formation.

Experimental Approach:

- Perform antibody-based fluorescence to determine molecular alterations in the heart of *Yap/Taz* deficient samples.
- Perform cardiac explant culture and *in-vitro* studies to validate cell fate decisions of *Yap/Taz* deficient neural crest cells.
- Perform unbiased sequencing and analysis to determine downstream targets of *Yap* and *Taz.*

Chapter 3: Methods

3.1 Generation of Transgenic Mouse Line

To generate NCC-specific deficiencies of Yap and Taz, *Wnt1-Cre; Yap$^{flox/+}$; Taz $^{flox/+}$* and *Wnt1-Cre2SOR; Yap$^{flox/+}$; Taz $^{flox/+}$* male mice were mated with *Yap$^{flox/+}$; Taz $^{flox/+}$* female mice and embryos were recovered from timed pregnancies. The *Wnt1-Cre; Yap$^{flox/+}$; Taz $^{flox/flox}$* and *Wnt1-Cre2SOR; Yap$^{flox/+}$; Taz $^{flox/flox}$* genotype served as the mutant embryos, *Wnt1-Cre; Yap$^{flox/+}$; Taz $^{flox/+}$* and *Wnt1-Cre2SOR; Yap$^{flox/+}$; Taz $^{flox/+}$* served as the double-heterozygous embryos, and all genotyping without *Wnt1-Cre* or *Wnt1-Cre2SOR* as controls. Generated transgenic mice were previously described, and contain the genetic background of B6-C57BL/6J [44]. Time mating was conducted and embryonic age was determined by the presence of a vaginal plug. Noon of the day the vaginal plug was observed was noted as embryonic day (E) 0.5. All animal experiments were approved by the University of Texas Health.

3.2 Histology and Hematoxylin and Eosin Staining

All embryos were dissected in phosphate-buffered saline (PBS) and fixed in formalin solution, neutral buffered, 10% (Sigma-Aldrich), and kept at 4ºC for 24 hours. Embryos were transferred to, and then kept in 70% ethanol at 4ºC the following day, or until needed. Samples were then embedded in paraffin. Embedded tissues were cut into 5 µm sections. Sectioned embryos, used for hematoxylin and eosin (H&E) staining, were first deparaffinized and rehydrated by use of HistoPrep-Xylene (Fisherbrand), followed by an ethanol series (100% to 75%). Sections were stained with hematoxylin (Sigma-Aldrich) for 6 minutes followed by water-acid ethanol and water-0.2% ammonium hydroxide rotations. Sections were then stained with Eosin-Y, 0.5% (Sigma-Aldrich)

for 30 seconds, followed by dehydration ethanal series (70% to 100%) and xylene. Slides were covered using Permount solution (Fischer Chemical). Images were taken using a Dmi8 S Platform Live cell microscope (Leica Microsystems) using the software Leica Application Suite X (Leica Microsystems).

3.3 EdU Staining and Immunohistochemistry

Before samples were harvested 0.5mg 5-ethynyl-2'-deoxyuridine (EdU) was injected intraperitoneally into pregnant dams, 2-3 hours before embryo collection. Embryos were harvested in PBS and fixed in formalin solution, neutral buffered, 10% overnight at 4ºC. Samples were transferred to 70% ethanol the following day and kept at 4ºC. For immunohistochemistry (IHC), samples were embedded in paraffin and sectioned at 5µm. Sectioned samples underwent a deparaffination protocol consisting of xylene and 70% to 100% ethanol series. Samples were submerged in 3% hydrogen peroxide for 15 minutes, followed by a heated antigen retrieval solution. Sections were blocked with PBS+Triton X solution (PBST) followed by 10% donkey serum in 0.5% PBST for 30 min, at room temperature. Sections were incubated with the primary antibody mouse-anti-actin, α-Smooth Muscle-Cyan3 (1:500; Sigma-Aldrich) overnight at 4ºC. The following day, sections were incubated with the secondary antibody donkey-anti-mouse 546 (Invitrogen, 1:200) for 2 hours at room temperature, followed by incubation with 4',6-Diamidino-2-Phenylindole, Dihydrochloride (DAPI) (ThermoFisher Scientific) for 30 minutes at room temperature. Slides were mounted using Fluoromount-G (SouthernBiotech) and 50mm glass coverslips (Globe Scientific Inc) and kept long-term at 4ºC. Fluorescence images were captured on a Zeiss confocal microscope with ZEISS ZEN microscope software.

3.4 Genotyping of Embryos

Tissue samples were collected simultaneously during embryo collection. Embryos were collected in PBS. Tissue from the tail was cut and used for genotyping from embryos collected at E14.5 through E18.5. For embryos at E9.5 and E10.5, the yolk sac and corresponding amnion were used for genotyping. All tissue taken was removed from the collection plate and washed in PBS in a separate dish, so as not to contaminate with blood or tissue from other samples or the female mouse. 200µl of 50mM sodium hydroxide (NaOH) was added to the tissue, and the mixture was heated at 95ºC - 99ºC for one hour by use of a heat-block. The tissue was homogenized every 20 minutes by flicking the tube. Followingly, 40µl of Tris pH 8.0 was added to the solution, and all was vortexed quickly and spun down for 2-3 minutes. Suspended DNA was either used immediately for polymerase chain reaction (PCR) or was stored at -20ºC. PCR was conducted using a normal and established protocol. A mixture containing 1µl of DNA and 19µl of master mix (42.1% H_2O, 52.6% PCR mix, 5.3% corresponding primers) is run for 30 denaturing-annealing-extending cycles, corresponding to pre-determined temperatures specific for the DNA of interest. Finalized product is mixed with EB Buffer (Alfa Aesar), and run for ~20 minutes at 180 volts on a ~1.5% agarose gel made with 0.5X TBE. Visualization is done with the use of a Gel Doc EZ Imager (Bio RAD).

3.5 TUNEL Assay

TUNEL assay was completed following an established protocol (Promega). Sectioned E9.5 embryos (sectioned at 5µm) first underwent a deparaffinization cycle (xylene followed by 100% - 70% ethanol series). Sections were then submerged in formalin solution, neutral buffered, 10% followed by incubation with Proteinase K solutions.

Positive controls were added for each sample tested. Positive controls were treated with DNase I for a total of 15 minutes, separately from test samples. All samples were incubated in equilibration buffer for 10 minutes followed by rTdT buffer (Terminal Deoxynucleotidyl Transferase, Recombinant) for 1 hour at room temperature. All sections were treated with 2XSSC for 15 minutes. Nuclei were stained using DAPI (1:500, ThermoFischer Scientific). Samples were mounted with Fluoromount-G (SouthernBiotech) and 50mm glass coverslips (Globe Scientific Inc), and then imaged using a Dmi8 S Platform Live cell microscope (Leica Microsystems) using the software Leica Application Suite X (Leica Microsystems).

3.6 O9-1 Cell Culture and siRNA Knockdown for Transwell Migration and Scratch Assay

O9-1 cells (Millipore Sigma, Catalog Number: SCC049) were cultured under un-differentiating conditions. Culture medium consisted of DMEM supplemented with 15% fetal bovine serum (FBS). The medium was conditioned with growth-inhibited STO (mouse embryonic fibroblast cell line) feeder cells (ATTC CRL-1503) overnight and filtered. For the siRNA knockdown, siRNA SMARTpools for control (Catalog Number: D-001810) or targeting *Yap* (Catalog Number: L-046247) and *Taz* (Catalog Number: L-041057) were purchased from Dharmacon and the transfections were performed, following a typical RNAiMAX transfection procedure (Invitrogen). For the scratch assay, O9-1 cells were seeded onto Matrigel Matrix (Corning, Product Number: 356234) diluted in DMEM, incubated for 2 hours at 37ºC, and covered with FBS for 1 hour at 37ºC. O9-1 cells were plated to create an even monolayer and incubated overnight in a 5% CO2, 37ºC incubator. siRNA for control or *Yap* and *Taz* was added

before incubation. A scrape was made on the cell monolayer using a p200 pipet tip. Dishes were placed in a 5% CO2, 37ºC incubator for a total of 240 minutes (4 hours) and images were taken every 30 minutes by use of a Zeiss microscope. For the transwell migration assay, O9-1 cells were seeded and allowed to get to 80% confluency in the basal medium. Once reached 80% confluency, cells were passed using basal medium containing 0.1% FBS and 1% LIF (Leukemia Inhibitory Factor, Millipore Sigma, Catalog Number: ESG1106). Transwell migration inserts were coated with Matrigel Matrix diluted in DMEM and allowed to solidify for 2 hours in a 5% CO2, 37ºC incubator. 600µl of basal medium containing 10% FBS was added to the well, and the Matrigel-coated inserts were placed inside each well. 100µl of O9-1 cells suspended in medium containing 0.1% FBS was added to the insert. 10µl of siRNA for control or *Yap* and *Taz* was added to the insert. Cells were incubated for 24 hours to allow for cell migration and siRNA knockdown. The following day, cells were fixed and immunofluorescence was performed using a primary antibody for Yap (1:200, Santa Cruz), followed by incubation with a donkey-anti-rabbit 488 secondary antibody (Invitrogen) and DAPI (1:500, ThermoFischer Scientific) to indicate nuclei. Imaging was completed using a Dmi8 S Platform Live cell microscope (Leica Microsystems) using the software Leica Application Suite X (Leica Microsystems).

3.7 *ex vivo* OFT Explant Culture

A solution of DMEM, supplemented with 10% FBS and 1% penicillin/streptomycin (100unit/mL and 100µg/mL, respectively), and 10% Matrigel was dispensed into 24-well microculture dishes and allowed to solidify at room temperature for 1 hour, followed by 30 minutes in a 37ºC, 5% CO_2 incubator. Cardiac outflow tracts (OFTs)

were harvested in sterile PBS from E10.5 embryos. OFTs were carefully dissected from the surrounding tissue and cut horizontally and then transferred to the Matrigel-covered wells using sterile plastic pipettes, to allow for attachment. Four hours after attachment to the Matrigel, 100µl of medium was added. Medium contains DMEM supplemented with 10% fetal bovine serum (FBS), 0.1% insulin-transferrin-selenium (ITS, Gibco, ThermoFisher Scientific), and 1% penicillin/streptomycin (100unit/mL and 100µg/mL, respectively) [70]. 150µl of medium was carefully replaced every 24 hours. Explants were cultured for a total of 4 days. Explants were fixed by use of formalin solution, neutral buffered, 10% at 4ºC, followed by incubation in PBST (PBS + 0.5% Triton X 100) for 15 minutes and blocking with 10% donkey serum in PBST for 1 hour, at room temperature. Immunofluorescence staining consisted of anti-actin, α-smooth muscle actin-Cyan3 (1:500; Sigma-Aldrich), overnight at 4ºC. The following day samples were incubated in the secondary antibody donkey-anti-mouse 546 (Invitrogen, 1:200) along with Alexa-Fluor 488 phalloidin (1:200; Invitrogen) for indicating F-actin. 4',6-Diamidino-2-Phenylindole, Dihydrochloride (DAPI) (ThermoFisher Scientific) was used for nuclei staining. Wells were covered using Fluoromount-G (SouthernBiotech) and kept at 4ºC. Fluorescence images were taken using a Dmi8 S Platform Live cell microscope (Leica Microsystems) using the software Leica Application Suite X (Leica Microsystems).

3.8 RNA Extraction for Ultra-low Bulk RNA-sequencing

RNA extraction was completed following the RNeasy Plus Micro Kit (Qiagen). The cardiac OFT was carefully dissected from E10.5 control and *Wnt1-Cre; Yap$^{f/f}$; Taz$^{f/f}$* embryos. OFTs were collected in sterile centrifuge tubes. A total of 350µl of Buffer

RLT Plus was added slowly (100µl - 150µl at a time), and homogenization took place using sterile pipette tips for 3-5 minutes to ensure that all tissue was separated. The lysate was transferred to a gDNA Eliminator spin column in a 2mL collection tube and centrifuged for 30 seconds, followed by adding 350µl of 70% ethanol to the flow-through and mixing by pipetting. All solution was transferred to an RNeasyMinElute spin column placed in a 2mL collection tube and centrifuged for 15 seconds. The spin column was saved and 700µl of Buffer RW1 was added, followed by centrifuging for 15 seconds. The flow through was discarded and 500µl of Buffer RPE was added to the spin column and centrifuged for 15 seconds. 500µl of 80% ethanol was added to the spin column and was spun down for 2 minutes. The spin column was left at room temperature for 10 minutes to allow the membrane to dry. Lastly, the membrane was rinsed with 14µl RNase-free water and spun down for 1 minute to release the RNA. Samples were used for Ultra-low Bulk RNA-sequencing only testing mRNA by the sequencing core at UTHealth. The control sample had an RNA concentration of 2,072.73 pg/µl (picogram/microliter) and the *Wnt1-Cre; Yap$^{f/f}$; Taz$^{f/f}$* sample had a concentration of 3,096.93 pg/µl.

3.9 Cell Counts and Statistical Analyses

Cell counts and expression levels were determined using ImageJ (Fiji). Corresponding data was transferred into GraphPad Prism 9 for statistical analysis and creation of the bar graphs. Quantitative data are presented as mean±SEM. Unpaired t test was used to compare 2 or more groups where $p<0.05$ was considered statistically significant (used for the analysis of IHC, TUNEL, OFT explant culture, scratch assay, and transwell migration assay). For bulk-RNA-sequencing data, raw counts were normalized to

fragments per kilobase million (FPKM) and we compared the log-2-fold-change (log2_FC) of the FPKM values between *Wnt1-Cre; Yap$^{f/f}$; Taz$^{f/f}$* and control. The plot of log2_FC from bulk-RNA-sequencing was created using R-studio ggplot package.

Chapter 4: Results

4.1 Yap/Taz Combinational Deficiencies in Neural Crest Cells Alters Cardiac Structure

In order to determine the function of *Yap* and *Taz* in NC-derived cardiac development, we bred mice accommodating floxed *Yap* and *Taz* genes (*Yap$^{f/f}$; Taz$^{f/f}$*, *Yap$^{f/+}$; Taz$^{f/+}$*) to mice containing the *Wnt1-Cre* or *Wnt1-Cre2SOR* drivers with floxed *Yap* and *Taz* genes (*Wnt1-Cre; Yap$^{f/+}$; Taz$^{f/+}$*, or *Wnt1-Cre2SOR: Yap$^{f/+}$; Taz$^{f/+}$*) to generate compound *Yap* and *Taz* conditional deficient embryos (*Wnt1-Cre; Yap$^{f/f}$; Taz$^{f/f}$*, *Wnt1-Cre; Yap$^{f/f}$; Taz$^{f/+}$*, *Wnt1-Cre; Yap$^{f/+}$; Taz$^{f/f}$*, *Wnt1-Cre; Yap$^{f/+}$; Taz$^{f/+}$*, *Wnt1-Cre; Yap$^{+/+}$; Taz$^{f/f}$*, *Wnt1-Cre; Yap$^{f/f}$; Taz$^{+/+}$*, *Wnt1-Cre2SOR; Yap$^{f/f}$; Taz$^{f/f}$*, *Wnt1-Cre2SOR; Yap$^{f/f}$; Taz$^{f/+}$*, *Wnt1-Cre2SOR; Yap$^{f/+}$; Taz$^{f/f}$*, *Wnt1-Cre2SOR; Yap$^{f/+}$; Taz$^{f/+}$*, *Wnt1-Cre2SOR; Yap$^{+/+}$; Taz$^{f/f}$*, *Wnt1-Cre2SOR; Yap$^{f/f}$; Taz$^{+/+}$*) [44]. Previous studies have found that the commonly used *Wnt1-Cre* can cause ectopic activation on *Wnt1*, particularly during midbrain development [84]. Although there has been no data indicating that there is ectopic expression of *Wnt1* in the cardiac region, we took the precaution to also include the *Wnt1-Cre2SOR* driver. However, during our investigation, we found that *Wnt1-Cre2SOR* displayed male germline activity in a small number of embryos collected (data not shown) [86]. To ensure our phenotypes were not affected by either possible Cre alteration, we excluded samples that displayed such variations from our study. We compared phenotypes between samples using either driver and found that overall, the phenotypic penetrance was similar at various

developmental time points. By use of both *Wnt1-Cre* and *Wnt1-Cre2SOR* drivers, the complete deletion of *Yap* and *Taz* (*Wnt1-Cre; Yap$^{f/f}$; Taz$^{f/f}$; Wnt1-Cre2SOR; Yap$^{f/f}$; Taz$^{f/f}$*) in pre-migratory NCCs resulted in embryonic lethality [44,45]. Furthermore, the complete deletion of *Yap,* in combination with a heterozygous deletion of *Taz* (*Wnt1-Cre; Yap$^{f/f}$; Taz$^{f/+}$, Wnt1-Cre2SOR; Yap$^{f/f}$; Taz$^{f/+}$*) also resulted in embryonic lethality around embryonic day (E) 10.5; however, an investigation into any cardiac development was not conducted [44]. We corroborated such conclusions in finding that samples with the complete deletion of either Yap or Yap/Taz, by use of either Cre driver (*Wnt1-Cre; Yap$^{f/f}$; Taz$^{f/+}$*; *Wnt1-Cre; Yap$^{f/f}$; Taz$^{f/f}$*; *Wnt1-Cre2SOR; Yap$^{f/f}$; Taz$^{f/f}$*; *Wnt1-Cre2SOR; Yap$^{f/f}$; Taz$^{f/+}$*) did not survive past E10.5. Due to such causality with the complete deletion of Yap in the NC, we mainly focused our investigation regarding cardiac morphology on samples that contained a *Yap* heterozygous deletion in combination with a *Taz* homozygous deletion (*Wnt1-Cre; Yap$^{f/+}$; Taz$^{f/f}$; Wnt1-Cre2SOR; Yap$^{f/+}$; Taz$^{f/f}$*), which we refer to as mutants, but for the investigation at developmental time points E9.5 we also gathered and investigated *Wnt1-Cre; Yap$^{f/f}$; Taz$^{f/+}$* and *Wnt1-Cre; Yap$^{f/f}$; Taz$^{f/f}$* embryos. Furthermore, we investigated the effects of a partial deletion of both *Yap* and *Taz* in the NC (*Wnt1-Cre; Yap$^{f/+}$; Taz$^{f/+}$*, *Wnt1-Cre2SOR; Yap$^{f/+}$; Taz$^{f/+}$*), which we refer to as double heterozygous samples. In contrast to samples with the complete deletion of *Yap,* we found that both mutant and double heterozygous embryos were able to survive through embryonic development (Table 1 and Table 2) and into postnatal developmental stages (data not shown).

To determine if Yap/Taz impacts cardiac development, we evaluated cardiac morphology from E10.5 through E18.5. At E18.5, mutant embryos displayed cardiac

defects such as an enlarged aorta (Figure 4B), great vessel mispositioning (Figure 4C), and a lack of aortopulmonary septation (Figure 4C), as compared to controls (Figure 4A). Similarly, at E16.5, mutant embryos, as compared to controls (Figure 5A), showed an enlarged aorta (Figure 5B) and mispositioning of the aortic trunk (Figure 5B-C). Mutant samples at E14.5 did not display obvious alterations to the external morphology of the heart (Figure 6B-C) and appeared grossly similar to controls (Figure 6A). Furthermore, no obvious defects of the cardiac outflow tract (OFT) were noted in mutants at E10.5 (Figure 7C-D) and E9.5 (Figure 8C-D), compared to controls (Figure 7A-B, Figure 8A-B). Lastly, we were able to investigate a*Yap/Taz* double homozygous (*Wnt1-Cre; Yap*$^{f/f}$*; Taz*$^{f/f}$*)* embryo at E10.5 and did not observe obvious alterations to the cardiac OFT (Figure 7E-F) when compared to controls (Figure 7A-B).

Embryonic Stage	Total Number of Samples	Total Number of *Wnt1-Cre; Yap$^{f/+}$; Taz$^{f/f}$*	Total Number of *Wnt1-Cre; Yap$^{f/+}$; Taz$^{f/+}$*	Total Number of Controls
E18.5	64*	7	9	41
E16.5	40*	4	10	26
E14.5	17*	2	1	11
E12.5	23*	2	3	15
E10.5	26**	4	3	17
E9.5	34*	3	5	22

Table 1: Total number of embryos using *Wnt1-Cre*

Embryos with the partial deletion of *Yap* and the complete inactivation of *Taz* were derived by crossing *Wnt1-Cre; Yap$^{f/+}$; Taz$^{f/+}$ males with Yap$^{f/f}$; Taz$^{f/f}$* or *Yap$^{f/+}$; Taz$^{f/+}$* females. Control embryos do not contain *Wnt1-Cre* but have a variety of *Yap* and *Taz* flox/flox combinations.

* There were dead embryos that could be genotyped
**There were dead embryos that could not be genotyped

Embryonic Stage	Total Number of Samples	Total Number of *Wnt1-Cre2SOR; Yap$^{f/+}$; Taz$^{f/f}$*	Total Number of *Wnt1-Cre2SOR; Yap$^{f/+}$; Taz$^{f/+}$*	Total Number of Controls
E18.5	50*	7	3	35
E16.5	15**	2	1	9
E14.5	13	2	1	9
E12.5	11*	0	1	4
E10.5	6	1	0	4
E9.5	15*	3	4	6

Table 2: Total number of embryos using *Wnt1-Cre2SOR*

Embryos with the partial deletion of *Yap* and the complete inactivation of *Taz* were derived by crossing *Wnt1-Cre2SOR; Yap$^{f/+}$; Taz$^{f/+}$ males with Yap$^{f/f}$; Taz$^{f/f}$* or *Yap$^{f/+}$; Taz$^{f/+}$* females. *Wnt1-Cre2SOR; Yap$^{f/+}$; Taz$^{f/f}$* embryos survived through E18.5. Control embryos do not contain *Wnt1-Cre2SOR* but have a variety of *Yap* and *Taz* flox/flox combinations.

* There were dead embryos that could be genotyped
**There were dead embryos that could not be genotyped

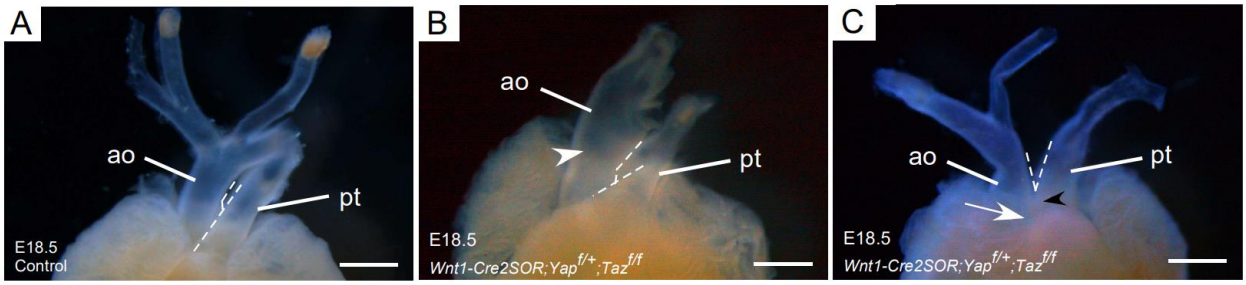

Figure 4: *Yap/Taz* mutant embryos display disrupted cardiac morphology at E18.5

Representative mutant hearts (using *Wnt1-Cre2SOR)* show an enlarged aorta, indicated by the white arrowhead (B), mispositioning of the aortic trunk, shown by the white arrow (C), and deficient aortopulmonary trunk septation, indicated by the black arrowhead (C), as compared to controls (A). Scale bar, 100µm. ao, aorta; pt, pulmonary trunk.

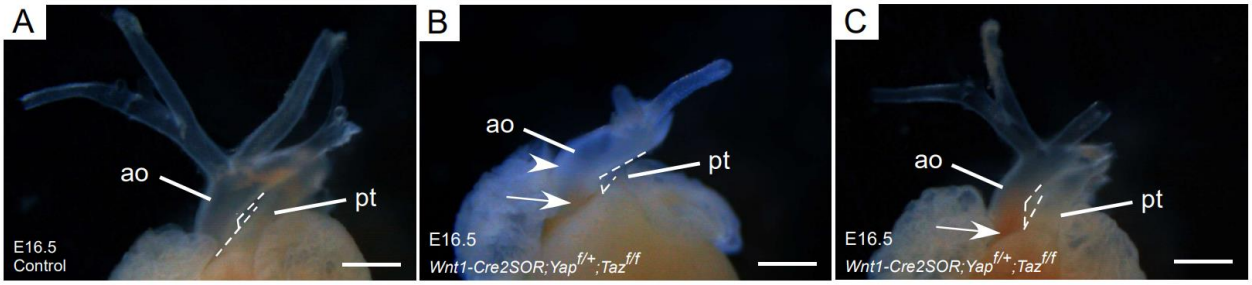

Figure 5: Main vessel defects in mutant embryos at E16.5

Representative mutant heart images (using *Wnt1-Cre2SOR*) show an enlarged aorta, shown by the white arrowhead (B), and mispositioning of the aortic trunk, indicated by the white arrow (B-C), compared to controls (A). Scale bar, 100µm. ao, aorta; pt, pulmonary trunk.

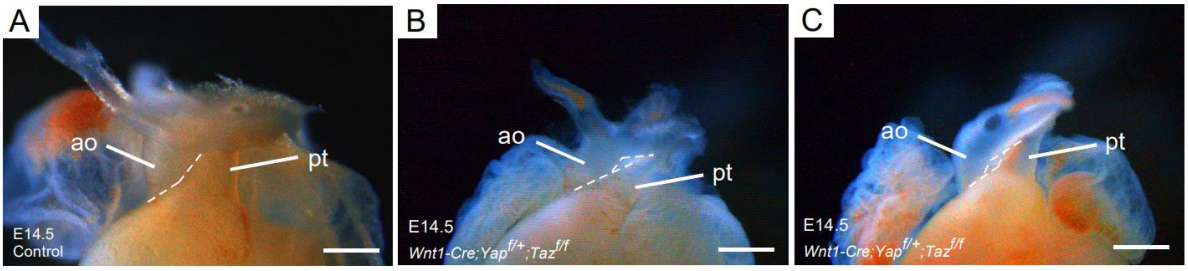

Figure 6: E14.5 mutant hearts do not have structural defects

Representative mutant heart images (using *Wnt1-Cre*) (B, C) show cardiac morphology similar to control images (A). Scale bar, 100µm. ao, aorta; pt, pulmonary trunk.

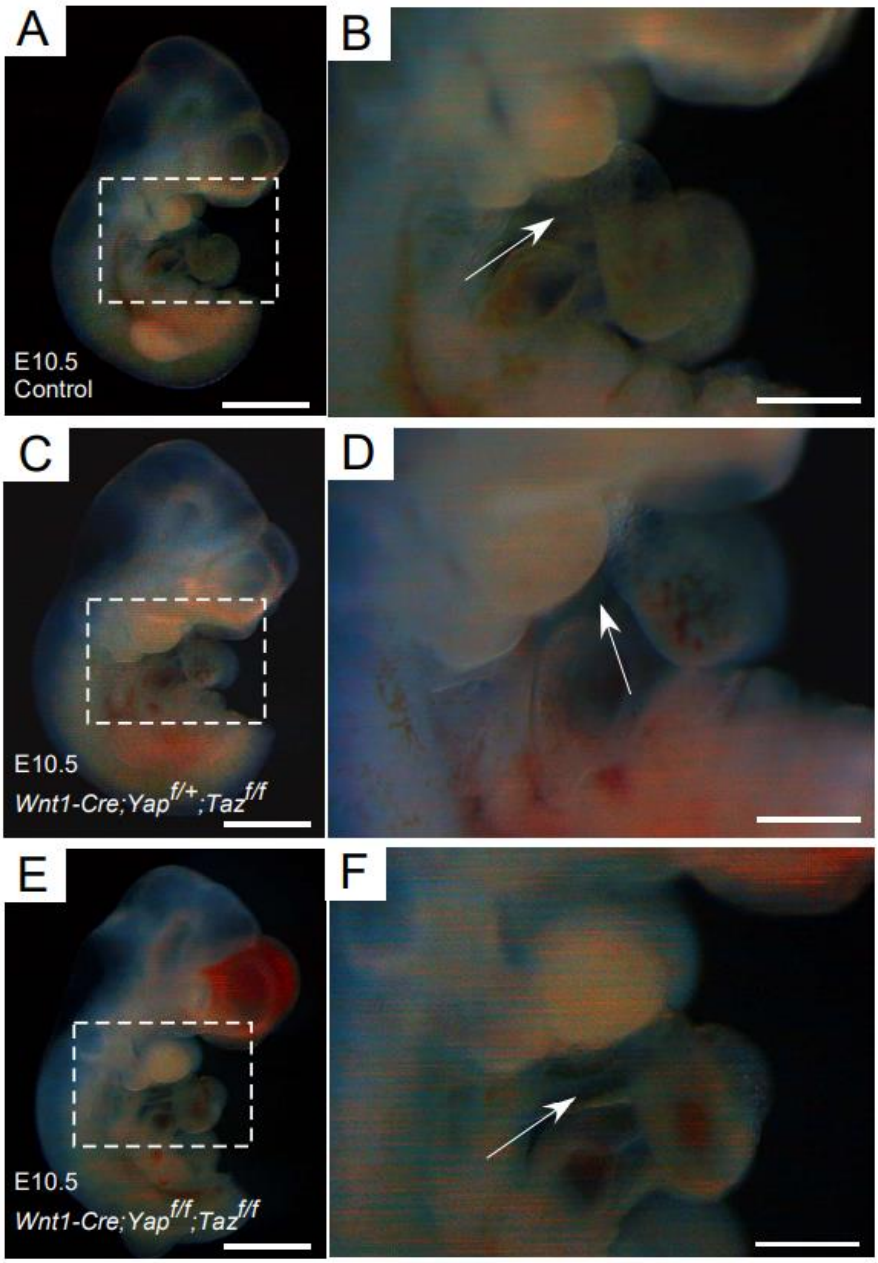

Figure 7: Cardiac outflow tract morphology is unchanged in mutant and double homozygous embryos at E10.5

Representative mutant (C, D) and *Yap/Taz* double homozygous (E, F) outflow tracts (OFTs) at E10.5 do not show obvious alterations when compared to controls (A, B). Panels on the right show higher magnification of the boxed area of panels on the left. OFT is indicated by white arrow (B, D, F). Scale bar, 100µm (A, C, E) and 500 µm (B, D, F).

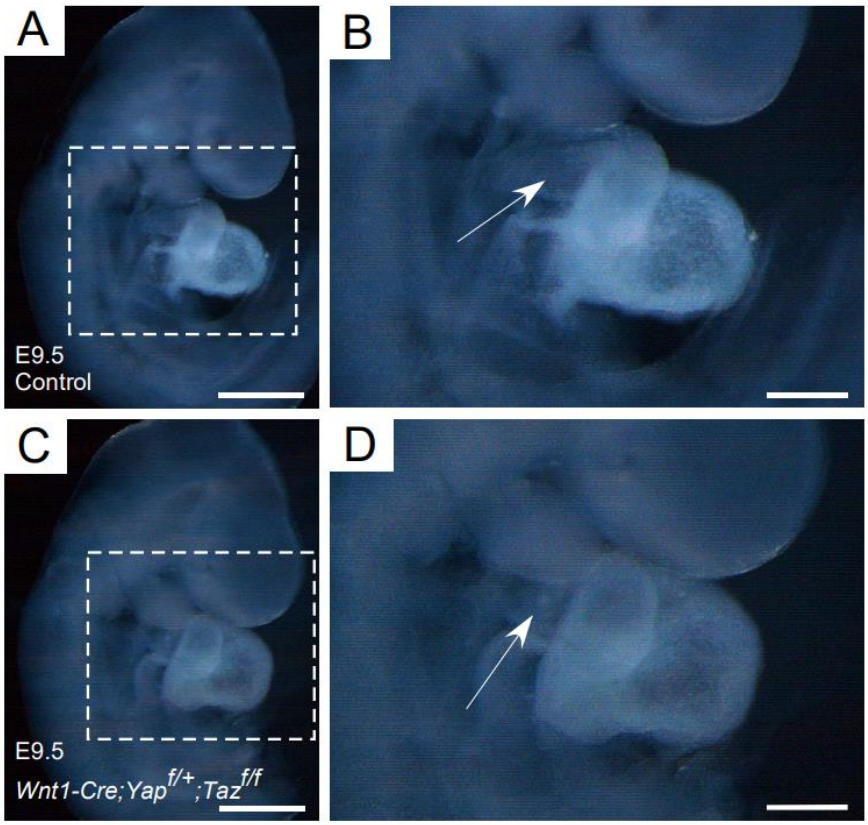

Figure 8: Cardiac outflow tract structure is unchanged in mutant embryos at E9.5

Representative mutant (C, D) outflow tract (OFT) at E9.5 do not show severe morphological alterations as compared with controls (A, B). Panels on the right show higher magnification of the boxed area of panels on the left. OFT is indicated by white arrow (B, D). Scale bar, 200μm.

Investigation into double heterozygous samples found that at E18.5, samples presented with minor aortic trunk mispositioning (Figure 9B), while one sample presented with pulmonary stenosis (Figure 9C), as compared to controls (Figure 9A). Similarly, E16.5 double heterozygous hearts presented with less severe cardiac alteration as compared with mutants, however, aortic trunk mispositioning was observed (Figure 10C) while a number of samples presented with no visible alterations (Figure 10B), as compared to controls (Figure 10A). E14.5 double heterozygous samples did not have altered morphology (Figure 11B) Furthermore, double heterozygous samples at E10.5 (Figure 12C-F) did not present with alterations of the

cardiac OFT, and presented with similar cardiac morphology as controls (Figure 12A-B).

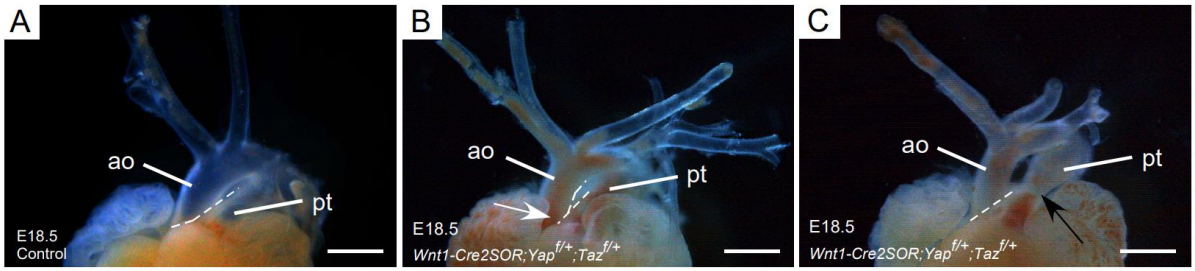

Figure 9: Double heterozygous embryos present with minor cardiac anatomy defects at E18.5

Representative double heterozygous heart images (using *Wnt1-Cre2SOR*) show minor mispositioning of the aortic trunk, indicated by the white arrow (B) and narrowing of the pulmonary artery, shown by the black arrow (C), as compared to controls (A). Scale bar, 100µm. ao, aorta; pt, pulmonary trunk.

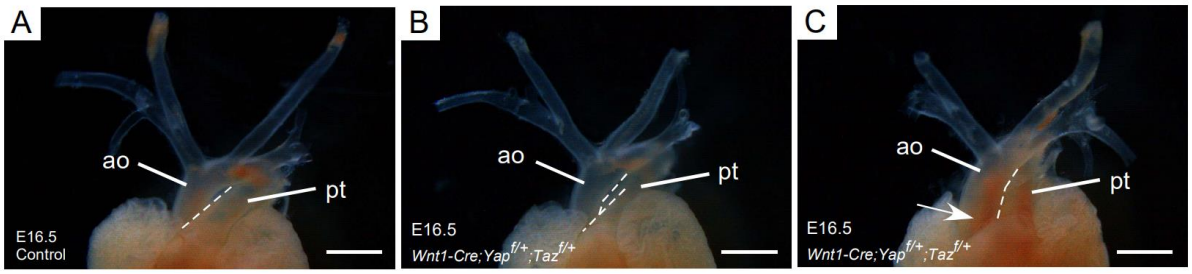

Figure 10: **E16.5 double heterozygous embryos have minor main vessel mispositioning**

Representative double heterozygous heart images (using *Wnt1-Cre*) show overall compare anatomy (B) to controls (A), however, a few double heterozygous hearts present with mispositioning on the aortic trunk, indicated by the white arrow (C). Scale bar, 100µm. ao, aorta; pt, pulmonary trunk.

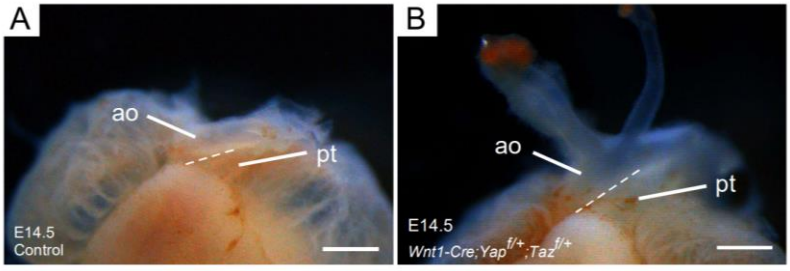

Figure 11: E14.5 double heterozygous embryos have no variation in cardiac structure

Representative double heterozygous heart image (using *Wnt1-Cre*) (B) shows cardiac morphology similar to control (A). Scale bar, 100µm. ao, aorta; pt, pulmonary trunk.

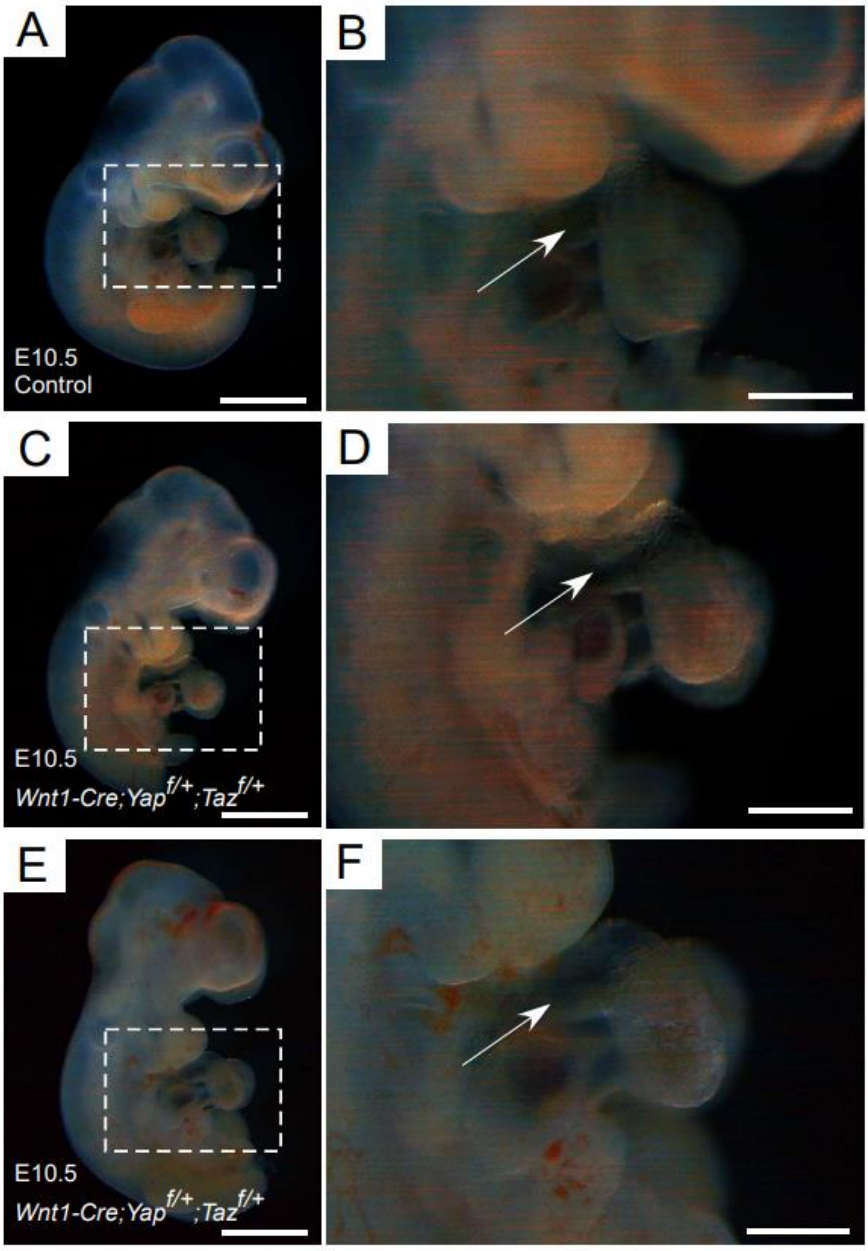

Figure 12: Outflow tracts of double heterozygous embryos at E10.5 have no structural defects

Representative double heterozygous heart images (using *Wnt1-Cre*) at E10.5 (C-F) show no variation between outflow tract (OFT) anatomy compared to controls (A, B). Panels on the right show higher magnification of the boxed area of panels on the left. OFT is indicated by white arrow (B, D, F). Scale bar, 100µm (A, C, E) and 500 µm (B, D, F).

4.2 *Yap/Taz* Combinational Deficiencies in Neural Crest Cells Alters Cardiac Anatomy

Cardiac NCCs are a significant contributor to OFT development and play a vital role in aorticopulmonary septation and OFT remodeling. To examine if *Yap/Taz* deficiencies in NCCs disrupted NC-derived internal cardiac structural formation, we performed histological examinations, using Hematoxylin and Eosin (H&E) staining. Histological analysis indicated that mutant embryos, compared to control embryos, presented with a variety of anatomical malformations. All mutant embryos at E18.5 presented with ventricular septal defect (VSD) (Figure 13B) when compared to controls (Figure 13A), while the majority of samples at this stage further displayed a range in severity of the phenotype double outlet right ventricle (DORV) (Figure 13D) (Table 4). Aortic valve leaflets of E18.5 mutants were found to be enlarged in mutant embryos (Figure 13B) as compared to controls (Figure 13A). Similarly, all E16.5 mutant embryos displayed VSD (Figure 14B) while most samples also displayed enlarged aortic valve leaflets (Figure 14B) compared to controls (Figure 14A), however, we do note that this enlargement at both E18.5 and E16.5 was not due to increased cell size. Furthermore, when compared to controls (Figure 14C), a number of E16.5 mutants presented with DORV (Figure 14D). The earliest display of VSD was discovered in E14.5 mutant samples (Figure 15B). However, E14.5 mutants, when compared to controls (Figure 15C), did not present with DORV (Figure 15D).

	Wnt1-Cre; Yap$^{f/+}$; Taz$^{f/f}$			*Wnt1-Cre; Yap$^{f/+}$; Taz$^{f/+}$*		
Embryonic Stages	**Ventricular Septal Defect**	**Aortic Valve Leaflet Enlargement**	**Double Outlet Right Ventricle**	**Ventricular Septal Defect**	**Aortic Valve Leaflet Enlargement**	**Double Outlet Right Ventricle**
E18.5	0/0	0/0	0/0	1/1	1/1	1/1
E16.5	4/4	3/4	2/4	2/2	0/2	0/2
E14.5	3/3	1/3	0/3	0/1	0/1	0/1

Table 3: Cardiac phenotypic rates of *Yap* and *Taz* alterations using *Wnt1-Cre* at different developmental stages

	Wnt1-Cre2SOR; Yap$^{f/+}$; Taz$^{f/f}$			*Wnt1-Cre2SOR; Yap$^{f/+}$; Taz$^{f/+}$*		
Embryonic Stages	**Ventricular Septal Defect**	**Aortic Valve Leaflet Enlargement**	**Double Outlet Right Ventricle**	**Ventricular Septal Defect**	**Aortic Valve Leaflet Enlargement**	**Double Outlet Right Ventricle**
E18.5	7/7	4/7	5/7	1/1	0/1	0/1
E16.5	1/1	0/1	1/1	0/0	0/0	0/0
E14.5	0/0	0/0	0/0	0/0	0/0	0/0

Table 4: Cardiac phenotypic rates of *Yap* and *Taz* alterations using *Wnt1-Cre2SOR* at different developmental stages

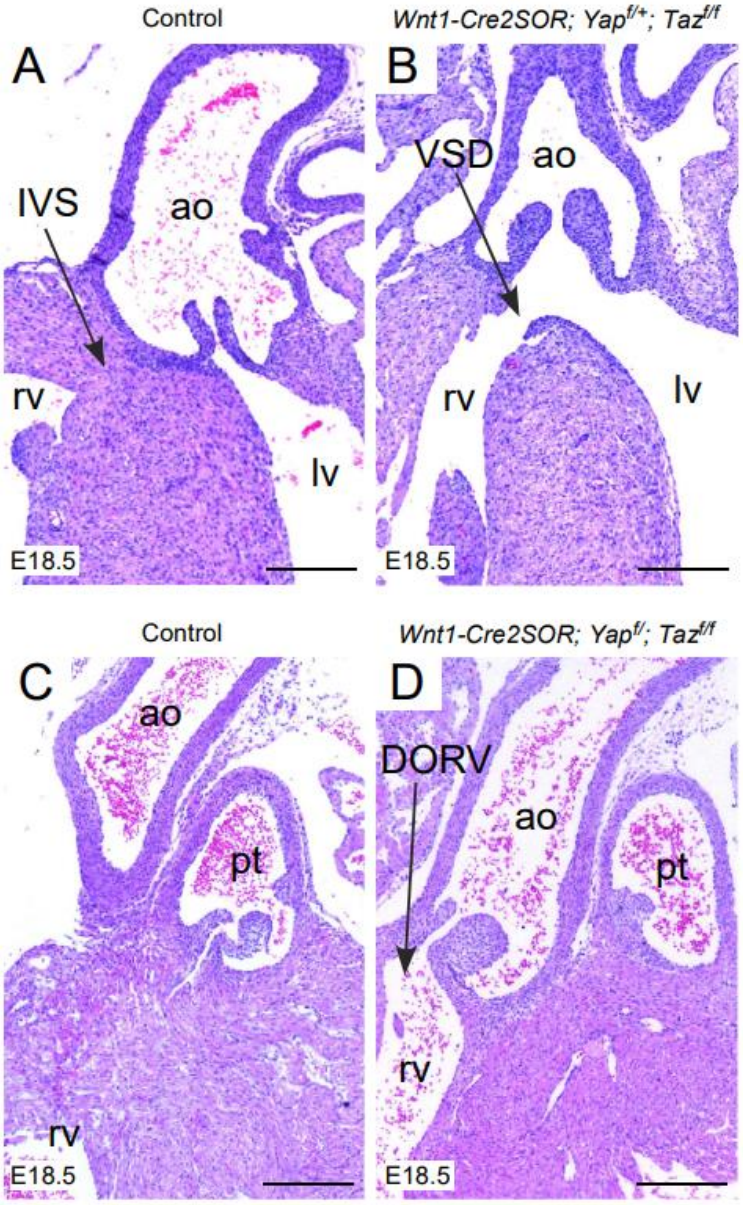

Figure 13: Sectioning reveals altered cardiac morphology in mutant embryos at E18.5

Embryonic hearts at E18.5 were dissected from the embryo. Hearts were embedded in paraffin and sectioned at 5µm. Hematoxylin and Eosin (H&E) staining was performed. Control hearts appear with normal anatomy consisting of an intact inter-ventricular septum (IVS) (A) and aortic trunk connection to the left ventricle (C). Mutant hearts present with ventricular septal defect (VSD) (B), enlarged aortic valve leaflets (B), and double outlet right ventricle (DORV) (D). Scale bar, 50µm. IVS, inter-ventricular septum; VSD, ventricular septal defect; DORV, double outlet right ventricle; rv, right ventricle; lv, left ventricle; ao, aorta; pt pulmonary trunk.

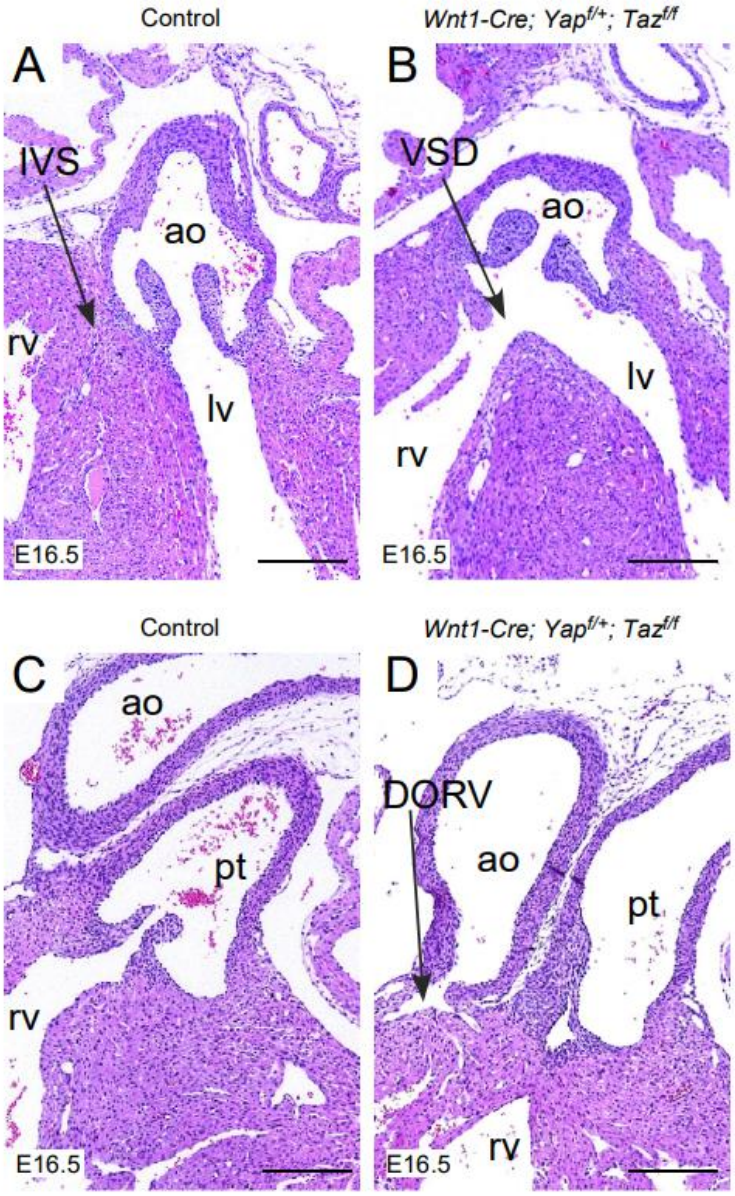

Figure 14: Various cardiac defects in mutant embryos at E16.5

Embryonic hearts at E16.5 were dissected from the embryo. Hearts were embedded in paraffin and sectioned at 5µm. Hematoxylin and Eosin (H&E) staining was performed. Control hearts appear with normal anatomy consisting of an intact inter-ventricular septum (IVS) (A) and aortic isolation to the left ventricle (C). Mutant embryos present with ventricular septal defect (VSD) (B), enlarged aortic valve leaflets (B), and double outlet right ventricle (DORV) (D). Scale bar, 50µm. IVS, inter-ventricular septum; VSD, ventricular septal defect; DORV, double outlet right ventricle; rv, right ventricle; lv, left ventricle; ao, aorta; pt pulmonary trunk.

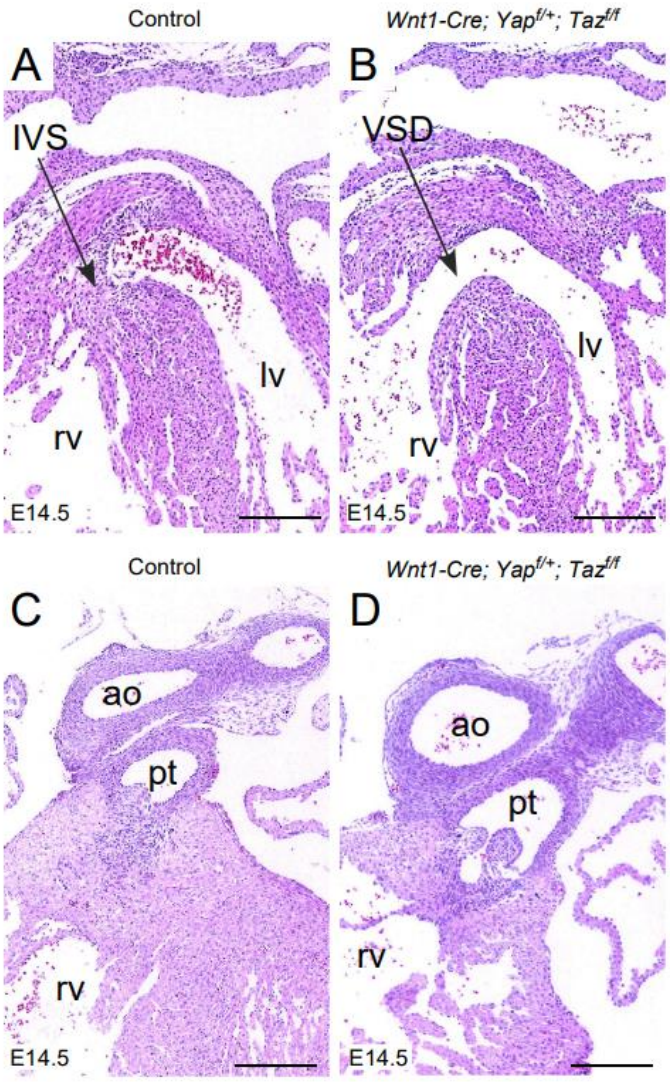

Figure 15: Ventricular septal defect is evident in mutant embryos at E14.5

Embryonic hearts at E14.5 were dissected from the embryo. Hearts were embedded in paraffin and sectioned at 5µm. Hematoxylin and Eosin (H&E) staining was performed. Control hearts appear with normal anatomy showing an intact inter-ventricular septum (VS) (A) whereas ventricular septal defect (VSD) can be seen in mutant embryos (B). Mutant hearts do not present with double outlet right ventricle (DORV) (D) and appear similar to control (C). Scale bar, 50µm. IVS, inter-ventricular septum; VSD, ventricular septal defect; rv, right ventricle; lv, left ventricle; ao, aorta; pt, pulmonary trunk.

Moreover, we investigated the anatomical development of Yap/Taz double heterozygous embryos, as compared to control embryos. At E18.5, a double heterozygous deficiency resulted in VSD (Figure 16B) when compared to controls (Figure 16A). Aortic valve leaflets of the double heterozygous heart appeared slightly misshapen at E18.5 (Figure 16B) when compared to controls (Figure 16A), however, do not appear as dramatically changed as mutant samples (Figure 13B). Furthermore, DORV was indicated at E18.5 (Figure 16D). At E16.5, double heterozygous hearts presented with minor VSD (Figure 17D) compared to controls (Figure 17C), however, did not display altered aortic valve leaflets (Figure 17B) which appear grossly similar to E16.5 controls (Figure 17A). Additionally, E16.5 double heterozygous hearts did not show DORV (Figure 17F) and again, appeared with similar cardiac structure to controls (Figure 17E). Lastly, E14.5 double heterozygous hearts mostly displayed cardiac anatomy similar to that of controls (Figure 18A, C). Double heterozygous hearts at E14.5 did not show DORV (Figure 18D) nor VSD (Figure 18B). However, we did note that E14.5 double heterozygous hearts showed what appeared to be weakened integrity of the membranous portion of the interventricular septum (IVS) (Figure 18B) compared to controls (Figure 18A), indicating a potential dose-dependent regulation of Yap and Taz for cardiac development.

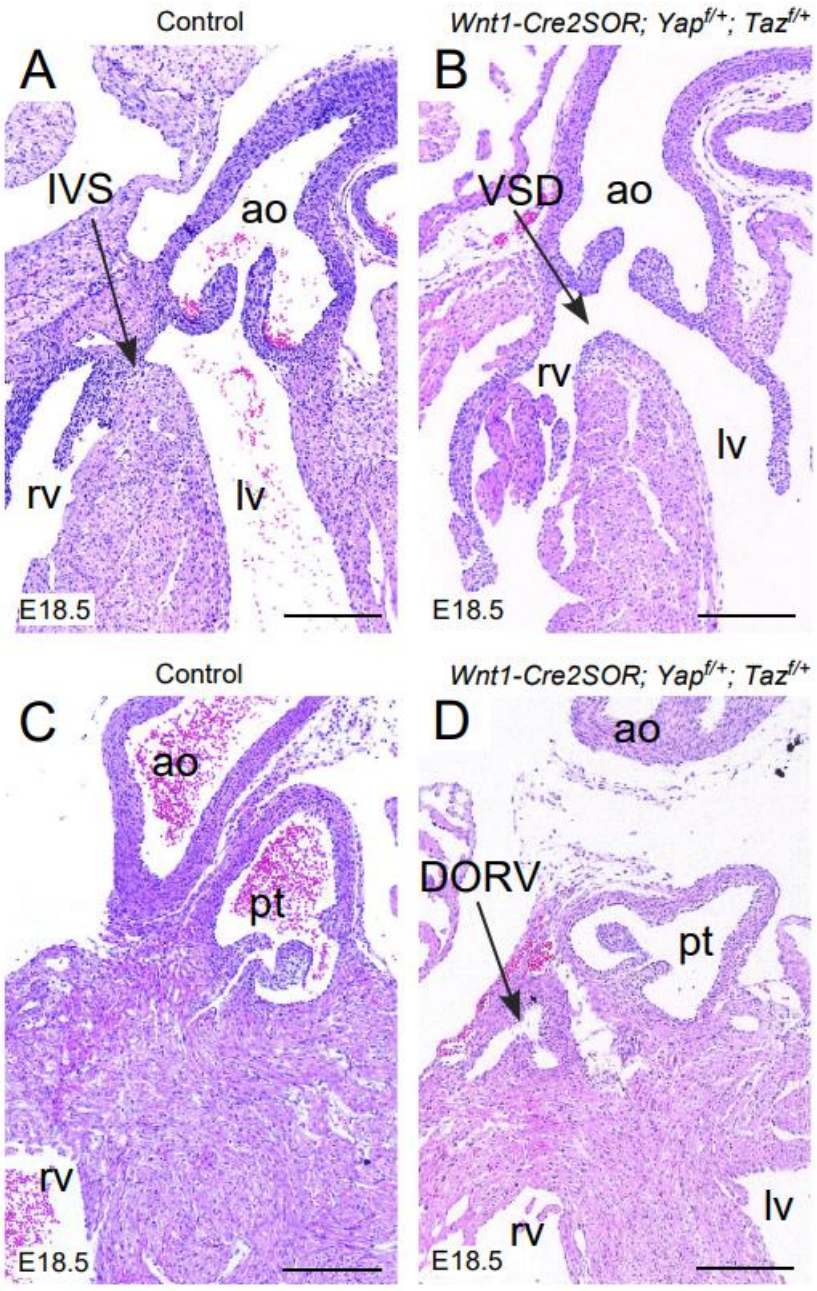

Figure 16: E18.5 double heterozygous hearts present with ventricular septal defect and double outlet right ventricle

Embryonic hearts were dissected from the embryo at embryonic stage 18.5. Hearts were embedded in paraffin and sectioned at 5µm. Hematoxylin and Eosin (H&E) staining was performed. Double heterozygous embryonic hearts show ventricular septal defect (B) and double outlet right ventricle (DORV) as compared to controls (A,C). Scale bar, 50µm. IVS, interventricular septum; VSD, ventricular septal defect; double outlet right ventricle; rv, right ventricle; lv, left ventricle; ao, aorta; pt, pulmonary trunk.

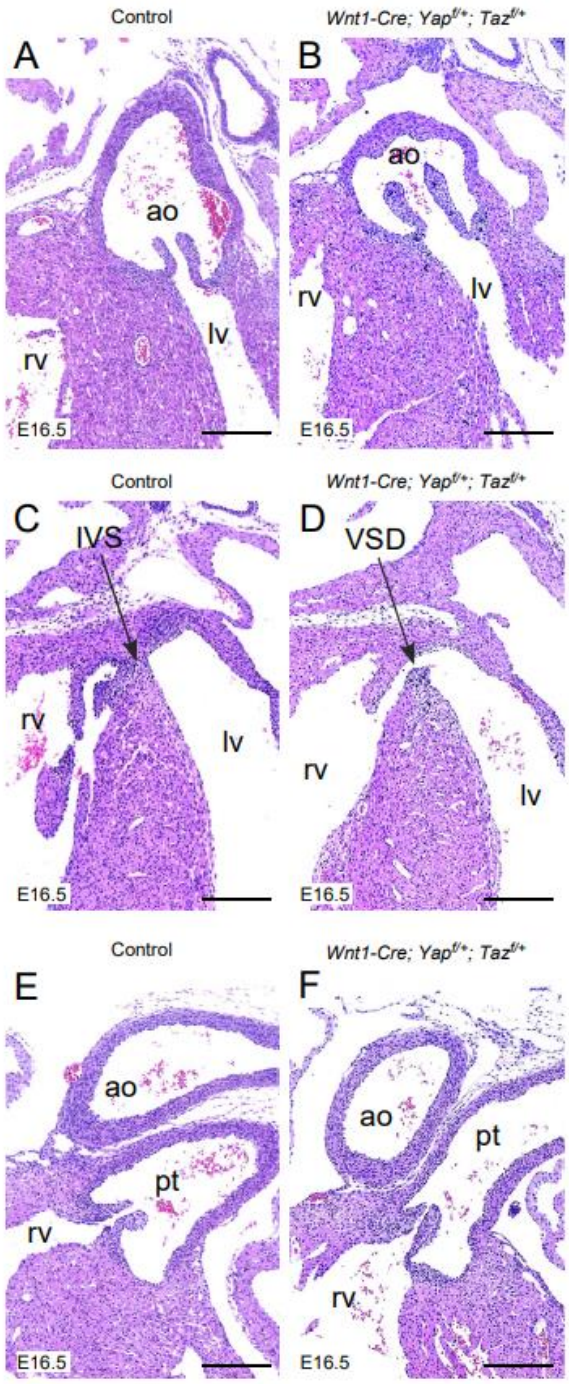

Figure 17: Sectioning reveals ventricular septal defect in double heterozygous hearts at E16.5

Embryonic hearts were dissected from the embryo. Hearts were embedded in paraffin and sectioned at 5µm. Hematoxylin and Eosin (H&E) staining was performed. Double heterozygous hearts show minor ventricular septal defect (VSD) (D) as compared to controls (C). *Wnt1-Cre; Yap*$^{f/+}$*; Taz*$^{f/+}$ hearts do not present with enlarged aortic valve leaflets nor double outlet right ventricle (DORV) (B, F), showing similar structure to controls (A, E). Scale bar, 50µm. IVS, interventricular septum; VSD, ventricular septal defect; rv, right ventricle; lv, left ventricle; ao, aorta; pt, pulmonary trunk.

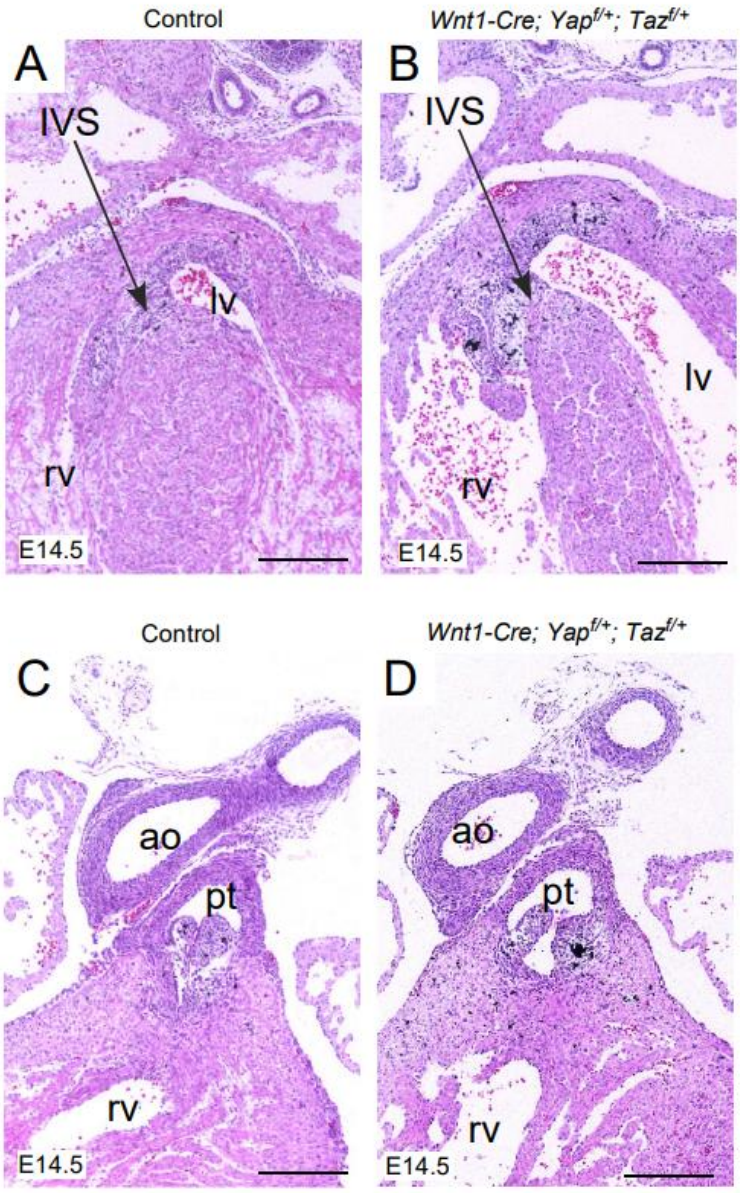

Figure 18: No cardiac defects in double heterozygous hearts at E14.5

Embryonic hearts were dissected from the embryo. Hearts were embedded in paraffin and sectioned at 5µm. Hematoxylin and Eosin (H&E) staining was performed. Double heterozygous hearts do not show ventricular septal defect (VSD) but structural integrity of the membranous portion of the interventricular septum (IVS) appears weakened (C) as compared to controls (A). *Wnt1-Cre; Yap$^{f/+}$; Taz$^{f/+}$* hearts do not present with double outlet right ventricle (D), and display similar morphology to controls (B). Scale bar, 50µm. IVS, interventricular septum; VSD, ventricular septal defect; rv, right ventricle; lv, left ventricle; ao, aorta; pt, pulmonary trunk.

4.3 Investigation into the Role of *Yap* and *Taz* in Neural Crest Cell Fate During Cardiac Development

To investigate if changes regarding NC-specific *Yap/Taz* expression alters dynamic cellular activity, we performed immunohistochemistry (IHC) studies of proliferation, differentiation, and cell apoptosis in control and mutant embryos. Due to anatomical phenotypes established by E14.5 (Figure 14), we focused our investigation regarding cell fate of the OFT at the earlier embryonic development stages of E9.5 and E10.5. We performed 5-ethynyl-2'-deoxyuridine (EdU) analysis for indication of cell proliferation and did not exhibit any obvious difference between control (Figure 19A-C) and mutant hearts (Figure 19D-F). Similar findings were found at E10.5, between mutants (Figure 20D-F) and controls (Figure 20A-C). Quantification of EdU-positive cells indicated that the rate of proliferation was unchanged in mutant embryos compared to control embryos at both E9.5 (Figure 19G-H) and E10.5 (Figure 20G-H).

In the OFT, cardiac NCCs differentiate into smooth muscle. To determine if this process occurs normally in the *Yap/Taz* mutant embryos, sagittal sections of E9.5 and E10.5 embryos were immunostained using an alpha-smooth muscle antibody (α-smooth muscle actin, aSMA), a differentiated smooth muscle cell marker. Staining showed no variation between α-SMA in the OFT of controls (Figure 22A-C) and mutant (Figure 22D-F) embryos at E10.5. At E9.5, no variation was found regarding the staining of smooth muscle expression of mutant (Figure 21D-F) and control (Figure 21A-C) embryos. In addition, quantification revealed that expression of aSMA in the OFT of mutant embryos was similar to the expression in the OFT of control embryos at E9.5 (Figure 21G-H) and E10.5 (Figure 22G-H), indicating that altered *Yap/Taz* in

NCCs does not affect proliferation nor smooth muscle differentiation during early cardiac development in the OFT.

To determine whether *Yap/Taz* deficiencies impact apoptosis in the OFT during early cardiac development, we performed TUNEL analysis in E9.5 *Wnt1-Cre; Yap$^{f/+}$; Taz$^{f/f}$* and control embryos. Our TUNEL data indicated that apoptosis was unchanged in the cardiac OFT of mutant embryos (Figure 23D-F) compared with controls (Figure 23A-C). The number of TUNEL positive cells in the OFT at E9.5 was extremely low, with some samples presenting with no positive signal in this region (Figure 24). Quantification of TUNEL positive cells in the OFT at E9.5 showed no variation between controls and mutants (Figure 23G-H). We note that TUNEL-positive cells were identified in other areas of the embryo, indicating that our analysis did work but that apoptosis is not present or altered in the OFT.

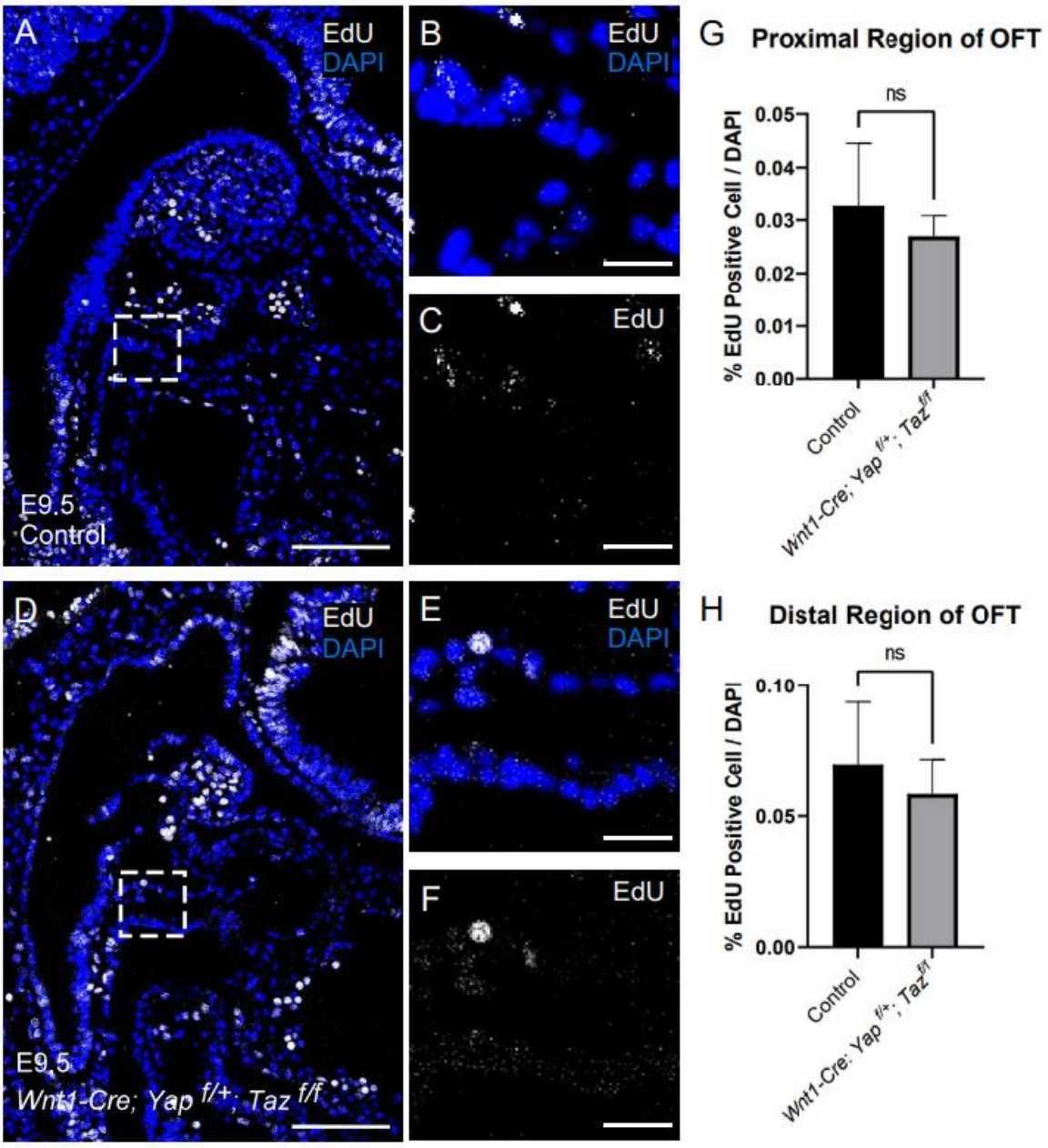

Figure 19: Proliferation rates are unchanged in the cardiac outflow tract of E9.5 mutant embryos

5-Ethynyl-2'-deoxyuridine (EdU) labeling (white) in the outflow tract (OFT) of control samples (A-C) presents with no significant variation when compared with EdU labeling of *Wnt1-cre; Yap$^{f/+}$; Taz$^{f/f}$* embryos (D-F). Nuclei are stained with DAPI (blue).

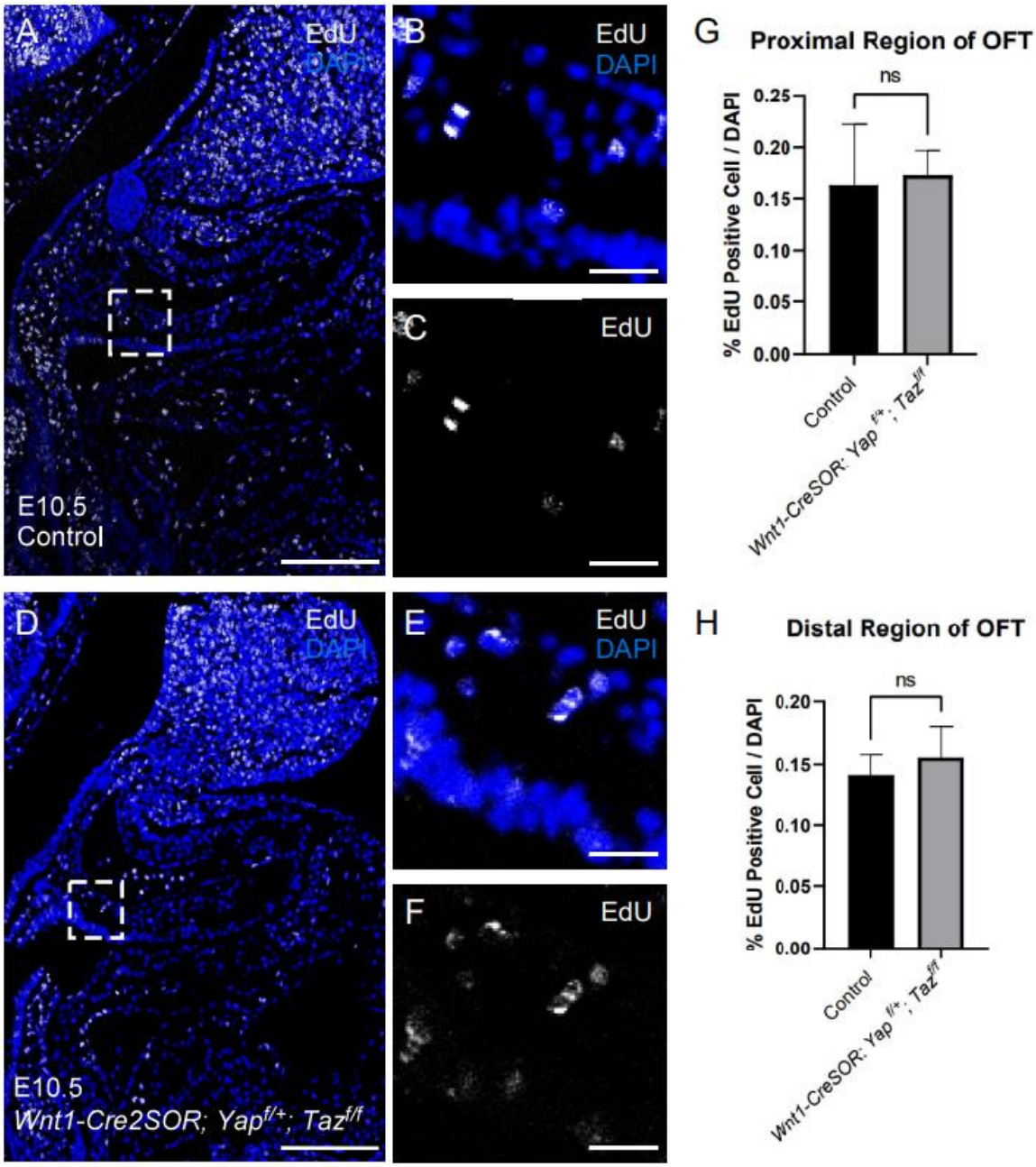

Figure 20: Proliferation rates are unchanged in the cardiac outflow tract of E10.5 mutant embryos

5-Ethynyl-2'-deoxyuridine (EdU) labeling (white) in the outflow tract (OFT) of mutant embryos (D-F) present with no significant variation when compared with EdU labeling of control samples (A-C). Nuclei are stained with DAPI (blue). Panels on the right show higher magnification of the boxed area of panels on the left. Statistical analysis of the amount of EdU positive cells in the distal (G) and proximal (H) regions of the OFT. $P<0.05$. All error bars represent s.e.m.

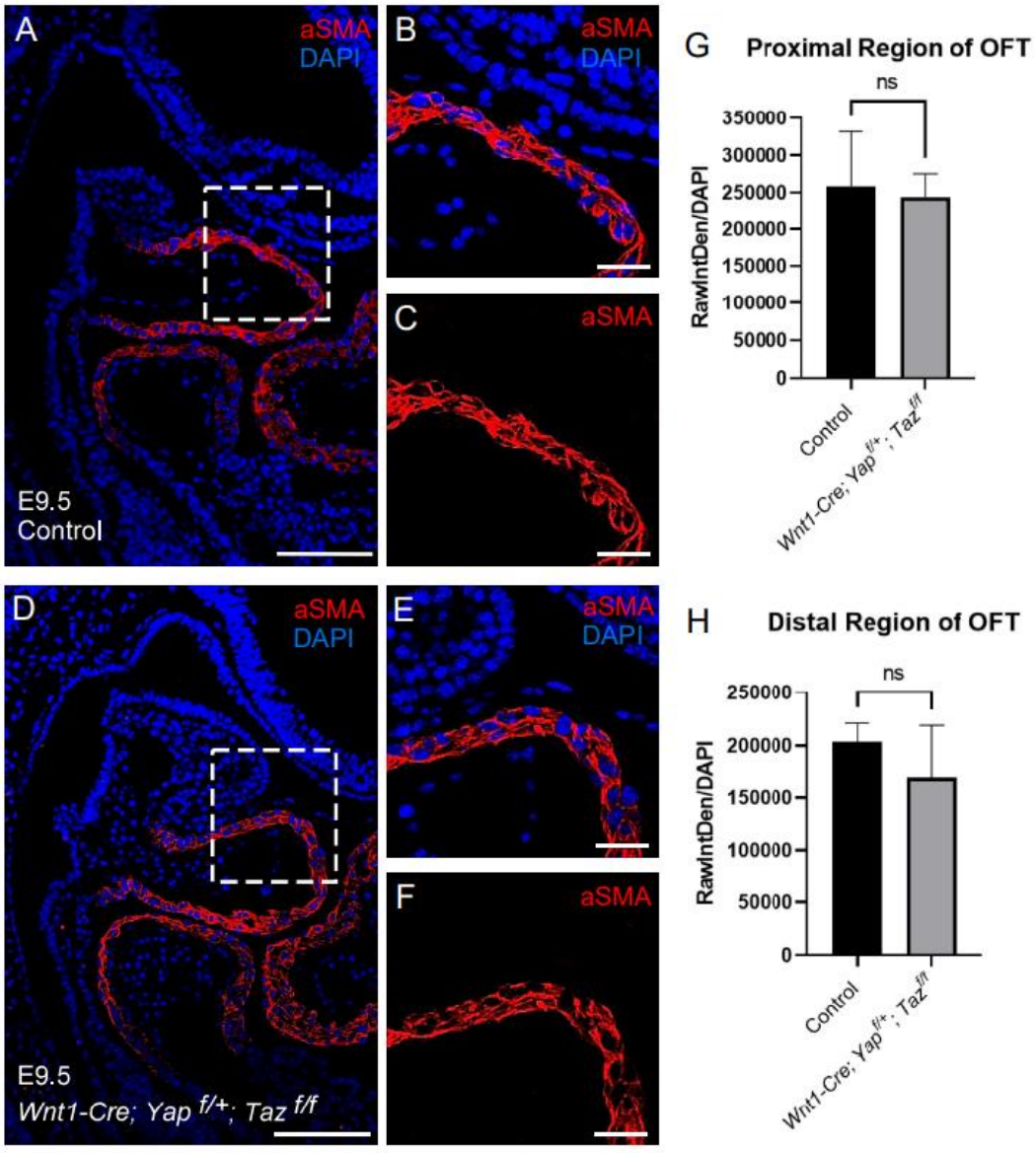

Figure 21: Smooth muscle differentiation is unchanged in the cardiac outflow tract of E9.5 mutant embryos

Compared with control embryos (A-C) *Wnt1-cre; Yap$^{f/+}$; Taz$^{f/f}$* embryos display similar smooth muscle expression in the outflow tract (OFT) at E9.5 (D-F). Smooth muscle cells are stained with aSMA antibody (red) and nuclei with DAPI (blue). Panels on the right (scale bar, 50μm) show higher magnification of the boxed area of panels on the left (scale bar, 200 μm). Quantification of aSMA expression intensity relative to the number of DAPI indicate no difference in smooth muscle between control and *Wnt1-Cre; Yap$^{f/+}$; Taz$^{f/f}$* embryos at both the distal and proximal regions of the OFT (G-H). $P<0.05$. All error bars represent s.e.m.

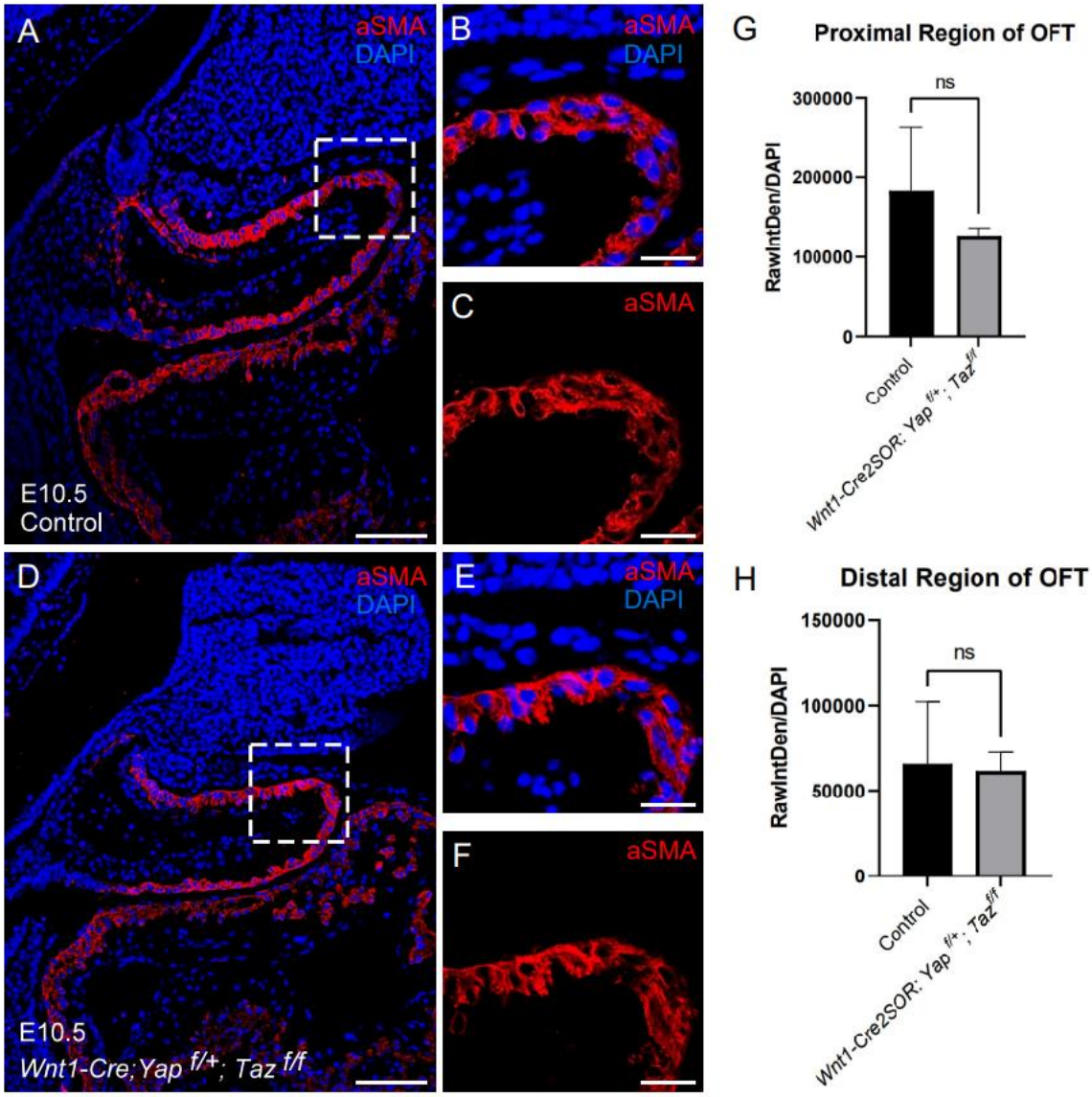

Figure 22: E10.5 mutant samples do not display altered smooth muscle differentiation in the cardiac outflow tract

Staining with aSMA antibody (red) for smooth muscle in control (A-C) and mutant embryos (D-F) indicates no variation of expression in the outflow tract (OFT) at E10.5. Nuclei are stained with DAPI (blue). Panels on the right (scale bar, 50μm) show higher magnification of the boxed area of panels on the left (scale bar, 200μm). Statistical analysis of the intensity of aSMA staining in the distal (G) and proximal (H) regions of the OFT, per the number of DAPI in the corresponding region, show no variation between samples. $P<0.05$. All error bars represent s.e.m.

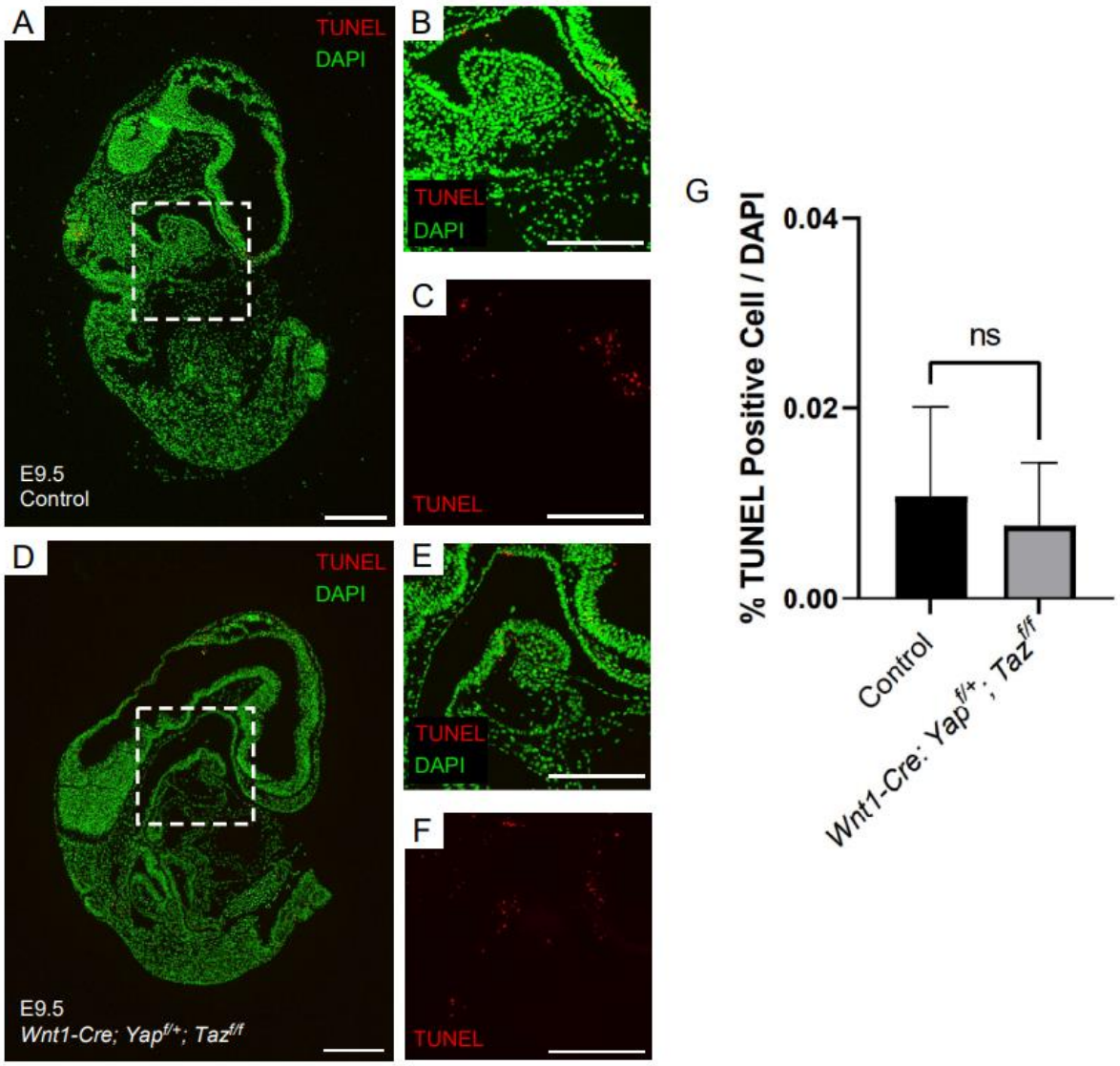

Figure 23: Apoptosis is unchanged in the outflow tract of E9.5 mutant samples

Immunofluorescence detection of apoptosis by TUNEL assay. The representative images of control (A-C) and *Wnt1-Cre; Yap$^{f/+}$; Taz$^{f/f}$* (D-F) embryos at E9.5 demonstrate similar proportions of TUNEL positive cells (red) in the cardiac OFT. Panels on the right show higher magnification of the boxed area of panels on the left. Scale bar, 200μm. Quantification of the number of TUNEL positive cells per the number of DAPI in the OFT shows no significance (G). $P<0.05$. All error bars represent s.e.m.

4.4 *Yap/Taz* Deficiencies in the Neural Crest Impair Cell Migration

One unique aspect of NCCs is their ability to migrate from the neural tube across the embryo during the early stages of embryogenesis. A previous study indicated the CKO of *Yap* and *Taz* in the NC did not alter NC migration or contribution to the OFT and development heart [45]. However, a detailed investigation using both *ex vivo* and *in vitro* models has not been conducted. To investigate if there is an effect on NC migration caused by *Yap* and *Taz* deficiencies, we cultured the OFT of E10.5 control and double heterozygous samples (*Wnt1-Cre; $Yap^{f/+}$; $Taz^{f/+}$)*. OFTs were allowed to culture on Matrigel-covered wells for 4 days. To calculate the total area cells were able to migrate, the area of the OFT tissue was subtracted from the area of all cells. This migrated area was then normalized by dividing by the area of the OFT tissue. We found that double heterozygous OFTs had a smaller area taken up by the migrated cells (Figure 24C) as compared to controls (Figure 24A). When we zoomed in, we could see that migrated cells from the control OFTs were larger (Figure 24B) when compared with migrated cells from the double heterozygous OFTs (Figure 24D). Furthermore, migrated cells from the double heterozygous OFTs were found to be clustered more tightly together (Figure 24D) than controls (Figure 24B). Quantification of the normalized total area OFTs cells were able to migrate was significantly less in double heterozygous samples (Figure 24E).

To specifically investigate the effects *Yap/Taz* deficiencies have on NCCs, we used the O9-1 cell line. The O9-1 cell line is a well-established and stable endogenous mouse embryonic stem cell population. These cells are originally derived from *Wnt1-Cre;* R26R-green fluorescent protein (GFP)-expressing cells and, under various conditions,

are able to differentiate into NC derivates including smooth muscle cells, osteoblasts, and chondrocytes [87]. To deplete the Hippo signaling pathway, we used siRNA-mediated knockdown to reduce the expression of *Yap* and *Taz* in O9-1 cells. Using deficient *Yap/Taz* O9-1 cells, we performed transwell migration and scratch assays to assess cell migration. Cell migration, of *Yap/Taz* deficient O9-1 cells, proved to be impaired (Figure 25D) during the scratch assay, as compared to controls (Figure 25C), over a period of 240 minutes (4 hours). Quantification of the number of cells that migrated past the initial boundary of the scratch, was significantly reduced in *siYap/Taz* treated cells compared with those treated with control siRNA (Figure 25E). Similarly, the percentage of O9-1 cells that were able to migrate across the membrane, in the transwell migration assay, was significantly less in cells treated with siRNA against *Yap* and *Taz* (Figure 26B, D) as compared to O9-1 cells treated with siRNA for control (Figure 26A, C). Quantification of the number of cells that were able to migrate across the membrane was significantly reduced for cells treated with siRNA for *Yap* and *Taz*, compared to control cells (Figure 26E).

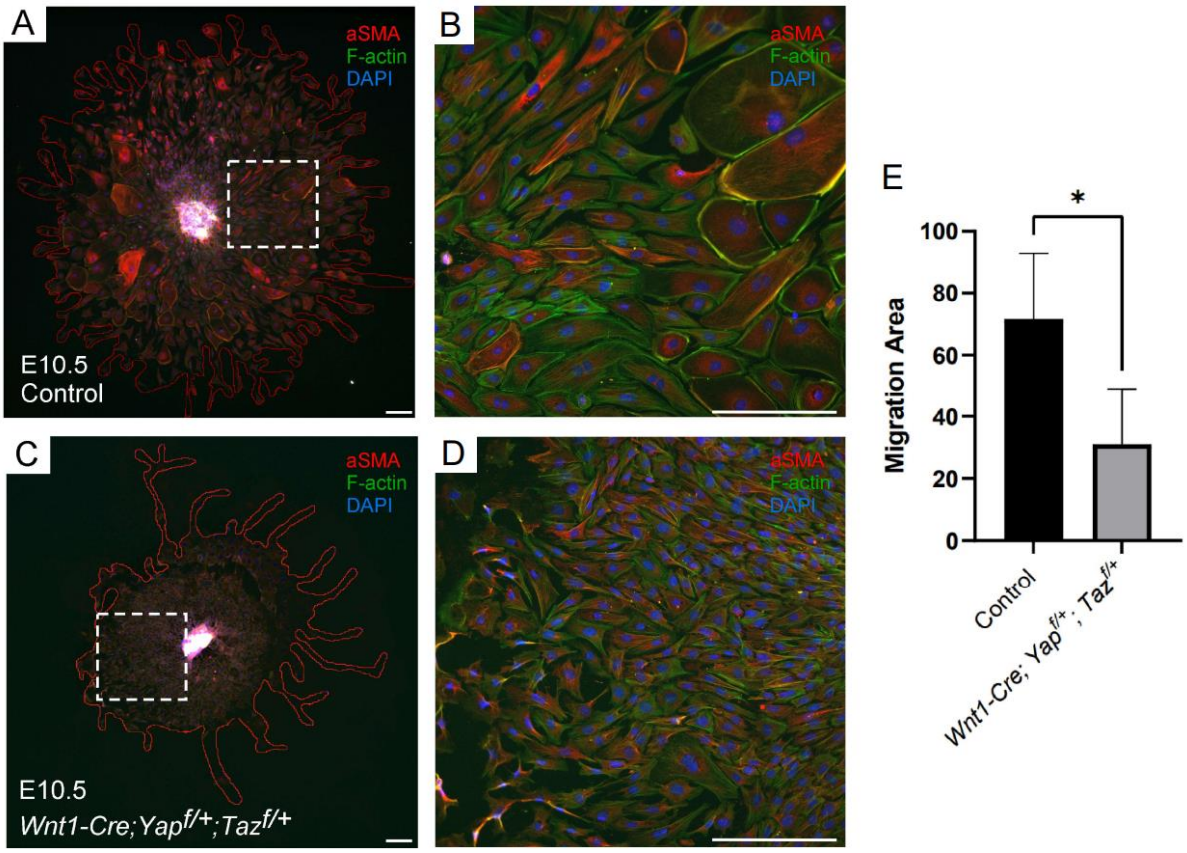

Figure 24: *ex vivo* migration assay of the cardiac outflow tract from double heterozygous embryos at E10.5 displays inhibited migration

OFT explants from E10.5 embryos of controls (A, B) and *Wnt1-Cre; Yap$^{f/+}$; Taz$^{f/+}$* (C, D) were dissected and cultured on Matrigel (outlined in red by use of FIJI-ImageJ software). OFTs were stained with alpha smooth muscle actin (aSMA, red) to indicate smooth muscle and phalloidin (F-actin, green) to indicate F-actin and visualize the cell shape. Panels on the right show higher magnification of the boxed area of panels on the left. Scale bar, 200µm. Quantification (E) indicates that the area cells were able to migrate was significantly reduced in *Wnt1-Cre; Yap$^{f/+}$; Taz$^{f/+}$* samples.

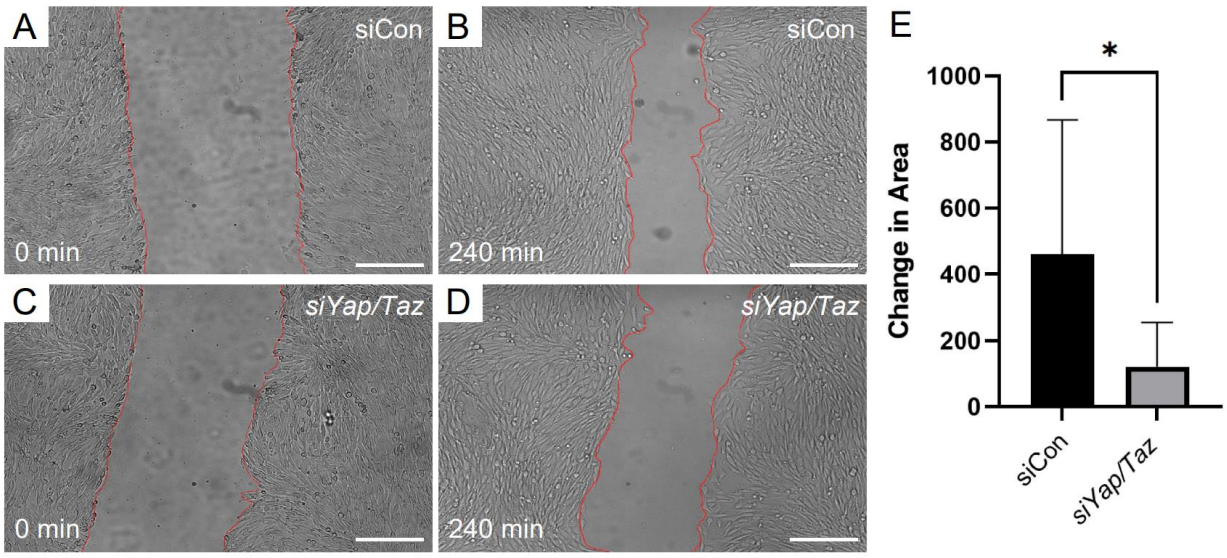

Figure 25: Inhibited O9-1 neural crest cell migration with deficiencies of *Yap* and *Taz*

O9-1 NC cells treated with siRNA for *Yap* and *Taz* migrated slower (D) as compared to cells treated with siRNA for control (B), over a 240-minute period. Quantification of the scratch area was found to be significantly smaller in controls cells compared with *siYap/Taz* treated cells (E). Scale bar, 200µm. $P<0.05$. All error bars represent s.e.m. siCon, siRNA control; *siYap/Taz*, siRNA *Yap* and *Taz.*

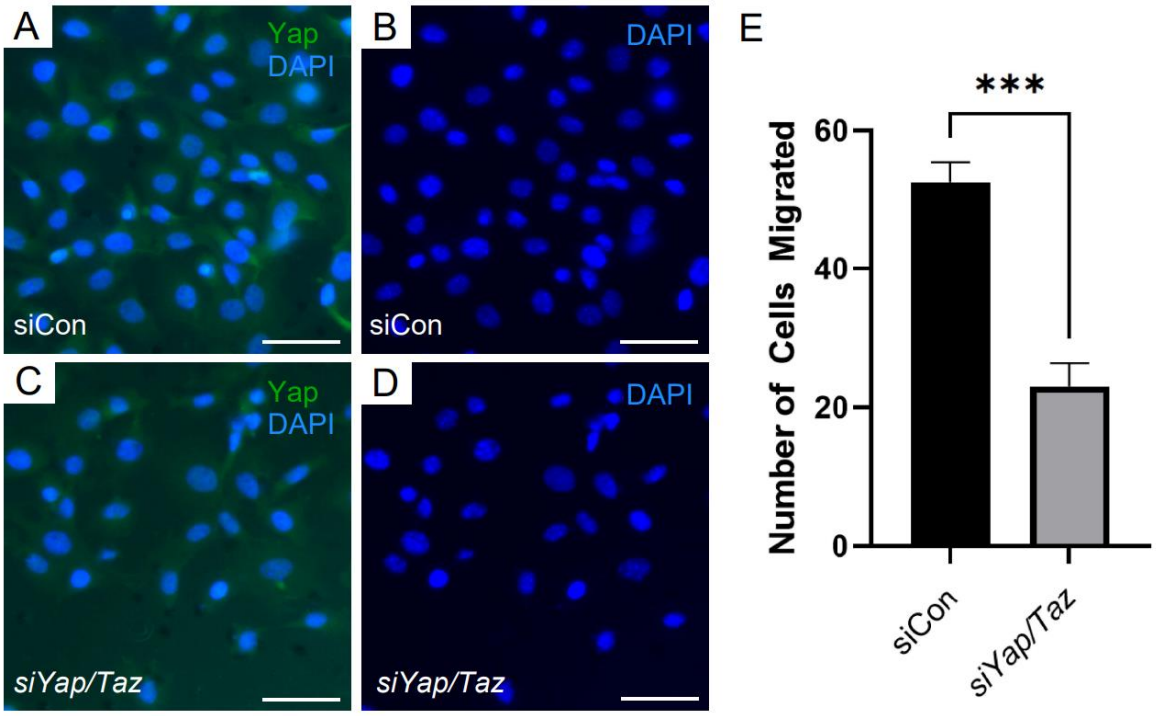

Figure 26: Inhibited migratory abilities of O9-1 cells with deficiencies of *Yap* and *Taz*

Fewer O9-1 NC stem cells treated with siRNA for *Yap* and *Taz* (C,D) were able to migrate compared to cells treated with siRNA for control (A,B) by use of transwell migration assay. Quantification of the number of cells able to migrate across the transwell membrane showed a significant reduction in siRNA for *Yap* and *Taz* treated cells (E). Scale bar, 50µm. $P<0.05$. All error bars represent s.e.m. siCon, siRNA control; *siYap/Taz*, siRNA *Yap* and *Taz.* Green, Yap antibody (Santa Cruz). Nuclei are stained with DAPI (blue).

4.5 RNA-sequencing Reveals a Role for the Hippo-Yap Pathway in Neural Crest Migration

Finding that the migration phenotypes are similar in both *ex vivo* and *in vitro* models, we focused our attention on the molecular mechanism underlying this migration phenotype. We performed Ultra-low-RNA-sequencing (Ultra-low-RNA-seq) analysis by using cardiac OFT RNA isolated from E10.5 *Wnt1-Cre; Yap$^{f/f}$; Taz$^{f/f}$* and control embryos. Gene ontology (GO) analysis of the Ultra-low-RNA-seq data revealed that extracellular matrix (ECM) organization and epithelial cell migration

were among the most highly downregulated GO terms (Figure 27). By use of the log-2-fold change (log2_FC) from our sequencing data set, along with our GO terms of interest, we identified a number of genes, associated with cell migration (Figure 28A) and ECM organization (Figure 28B) that had a log2_FC less than -2 and -1.5, respectively. Genes related to ECM organization include, Col1a1, Col2a1, Col5a1, Col9a1, Col9a2, Col11a1, Col12a1, Col22a1, Tgfbi, Lamb3, Lum, and Ltbp4 (Figure 28B). Genes related to cell migration include, Fgf1, Fgf8, Bmp4, Gata2, Twist2, Jam2, Nbl1, Thbs1, Hdac9, Wnt4, Wnt11, Ptprr, and Sema3c (Figure 28A).

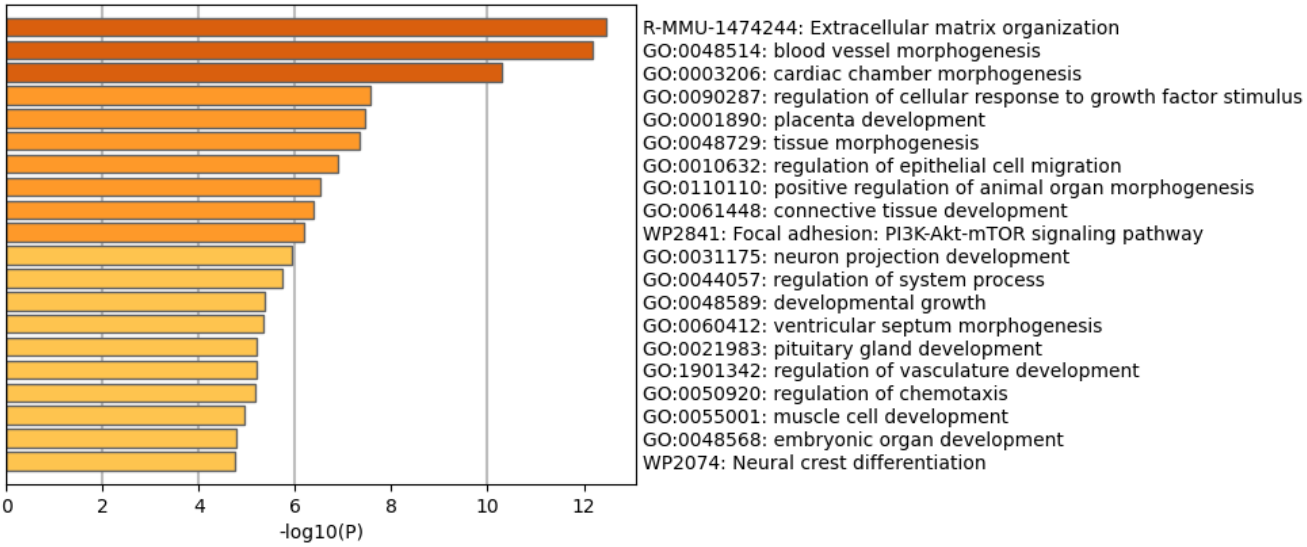

Figure 27: GO term analysis reveals downregulated terms from Ultra-low Bulk RNA-sequencing

Gene ontology (GO) term enrichment analysis of genes with a log2 fold change (log2_FC) less than -1.5 from Ultralow-Bulk-RNA-sequencing, comparing tissue of the cardiac OFT between *Wnt1-Cre; Yap*$^{f/f}$*; Taz*$^{f/f}$ and control at E10.5.

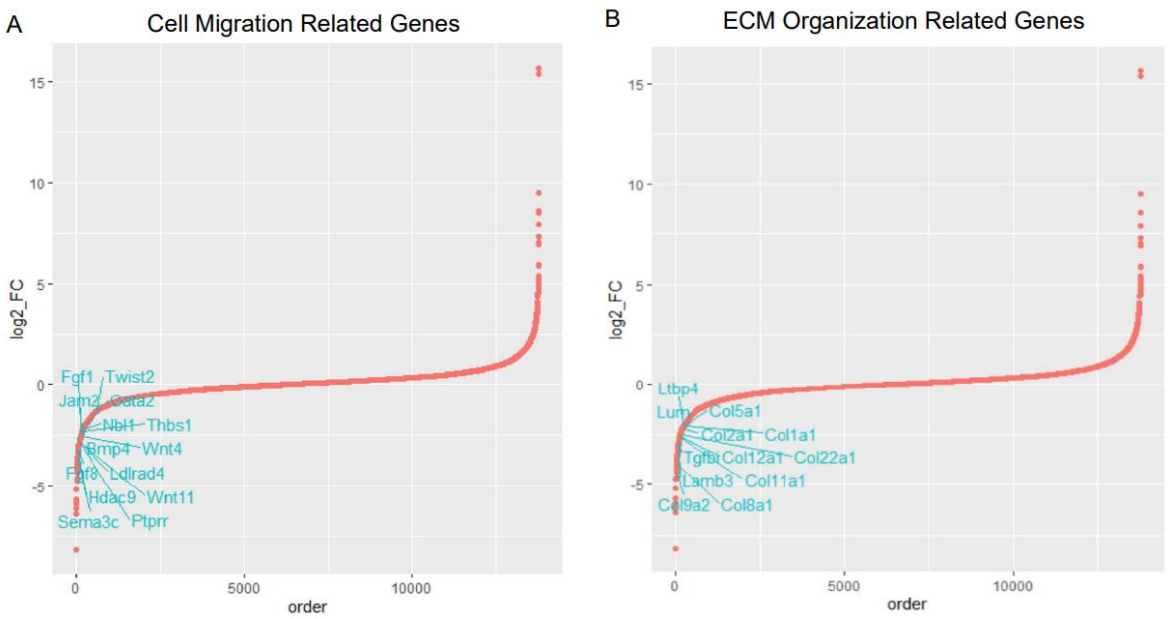

Figure 28: Downregulation of cell migration and ECM organization genes

Plot of log2-fold change (log2_FC) of the fragments per kilobase million (FPKM) from Bulk RNA-seq of E10.5 control and *Wnt1-Cre; Yap*$^{f/f}$*; Taz*$^{f/f}$ OFTs. Y-axis represents the log2_FC and x-axis represents ordering of the log2_FC. (A) Genes listed in blue are associated with cell migration, and presented with a log2_FC less than -1.5. (B) Genes listed in blue are associated with extra-cellular matrix organization and cell-cell adhesion, and presented with a log2FC less than -2. Plots made using R-studio.

Chapter 5: Discussion, Future Directions, and Conclusions

5.1 Discussion

The Hippo signaling pathway is a highly-conserved kinase cascade that has important roles in tumorigenesis, tissue regeneration, embryogenesis, and organogenesis [88-93]. Although evidence suggests that the Hippo signaling pathway plays a role in cardiac cell fate, there are still no studies to provide insight into this pathway's role through the neural crest (NC) for heart development. The heart is derived from various populations of cells contributing to specific cardiac components. Neural crest cells (NCCs) are derived from the neural tube and contribute to the cardiac outflow tract (OFT), later assisting in aorticopulmonary septation, and the membranous portion of the interventricular septum (IVS) [7,9,17]. However, the improper contribution of these cells can alter cardiac formation leading to various congenital heart defect (CHD) phenotypes [7,9,16]. Our study demonstrated that the inhibition of *Yap* and *Taz* in the NC population impairs heart development. Although cardiac defects varied slightly in the severity between embryonic stages, all mutant samples (*Yap* heterozygous and *Taz* homozygous deletions) at embryonic stages (E) 14.5, E16.5, and E18.5 presented with ventricular septal defect (VSD), one of the most common CHD phenotypes observed in humans [56]. Although not observed as frequently as VSD, double outlet right ventricle (DORV) was also found at both E16.5 and E18.5, along with enlargement of the aortic valve leaflets. We corroborate the findings presented by Wang et. al. (2016) and Manderfield et. al. (2015), who demonstrated that samples with the complete deletion of both *Yap* and *Taz* by the use of *Wnt1-Cre* or *Wnt1-Cre2SOR*, did not survive past E10.5 [44,46]. Furthermore, we found that the severity of such

cardiac defects may be correlated to the levels of Yap and Taz in the NC. Using both *Wnt1-Cre* and *Wnt1-Cre2SOR,* we created double heterozygous deficient embryos. We found that the penetrance of cardiac defects observed was overall lower in the double heterozygous embryos compared to mutant embryos. We also found that although double heterozygous samples did present with phenotypes similar to mutants, such as VSD, the phenotype itself was less severe. Previous studies have concluded that NC ablation results in similar cardiac defects during embryogenesis, however no study to date has investigated the Hippo-Yap signaling pathway's contribution. Our study establishes a role of Yap and Taz in NC-derived cardiac development.

Alongside our results demonstrating the necessity for Yap and Taz in NC-derived heart formation, we provide evidence that during early cardiac development, specifically at E9.5 and E10.5, Yap/Taz have a role in migratory cell fate decisions. However, we also investigated other aspects of cell fate including differentiation, proliferation, and cell death. Regarding differentiation, we found that smooth muscle expression in the OFT, indicated by alpha-smooth muscle immunohistochemistry staining, was not altered in both the distal and proximal regions. This contradicts previous findings that reported that the double-conditional deletion of *Yap* and *Taz* in the NC significantly reduced smooth muscle expression in the third aortic arch artery [45]. Such variations in results may be due to the difference in gene composition or that the investigation into smooth muscle differentiation took place in varying components of the heart. Similar to our findings that smooth muscle differentiation in the OFT is unchanged in *Yap/Taz* mutant embryos, our results further suggest no variation in the number of proliferating cells or the number of cells undergoing apoptosis. Regarding

cell proliferation in the OFT, these results support previous findings of Manderfield et. al. (2015), who determined that the complete deletion of both *Yap* and *Taz* in the NC population does not alter the number of proliferating cells in the third arch artery [45]. We further concluded that in the OFT, the number of apoptotic cells was unchanged. Although previous studies have not investigated cell death in the heart of *Yap/Taz* deficient embryos, Wang et. al. (2016) found that in the mandible of embryos with the complete deletion of both *Yap* and *Taz* in the NC, the number of cells undergoing apoptosis was significantly greater compared to controls [44]. However, Manderfield et. al. (2015) concluded that *Yap/Taz* complete deletion embryos did not display detectable changes in the number of apoptotic cells in the neural tube [46]. Lastly, regarding cell fate in the cardiac OFT, we investigated cell migration. NCCs are known for their migratory capabilities, as this is vital for their contribution to the developing embryo. By use of *ex vivo* culture of the cardiac OFT from E10.5 *Yap/Taz* double heterozygous and control embryos, our results demonstrate that *Yap/Taz* deficiency in the NC impedes cell migration. We further validated our *ex vivo* findings by using the O9-1 NCC line. Through the completion of scratch and transwell migration assays, we corroborated our previous conclusion that a deficiency of *Yap* and *Taz* in NCCs inhibited cell migration. However, a general consensus on the role Yap/Taz has on cardiac NCC fate, regarding differentiation, proliferation, death, and migration, during heart development has yet to be conclusively defined.

Finally, our unbiased bulk-RNA-sequencing data identified that cell migration and extracellular matrix (EMC) components were of the most downregulated terms from OFTs of *Yap/Taz* complete deletion embryos compared to controls. From the

identified downregulated Gene Ontology (GO) terms, we identified several genes that presented with a significantly downregulated fold-change. Although the majority of the identified genes have not yet been directly correlated with either NC migration or the Hippo-YAP signaling pathway specifically, our results demonstrate the potential for novel downstream targets of Yap/Taz for NC migration.

5.2 Future Directions

Although we have uncovered a role for *Yap* and *Taz* in NC-derived cardiac development and cell migration, more work is needed to properly identify the full effects *Yap/Taz* have on cardiac morphology.

From our study, we concluded that *Yap/Taz* mutant embryos did not display altered cell proliferation, apoptosis, or smooth muscle differentiation in the OFT. However further investigation is needed regarding the complete deletion of both *Yap* and *Taz* in the NC population, and its effects on early cardiac development, despite being embryonically lethal. Regarding cell migration, *ex vivo* studies should be further conducted using *Yap/Taz* mutant and complete deletion embryos. Although our *ex vivo* study provided novel insight into cell migration in the OFT, we cannot disregard entirely the possibility that *Yap/Taz* deficiency alters NC migration and delamination from the neural tube to the OFT. To gain a better understanding of the role Yap/Taz have on NC migration, live-imaging using a tracer, such as a green-fluorescent protein (GFP) reporter, would provide a concise conclusion of cell migration *in vivo.* Furthermore, live-imagining with a tracer would provide supporting evidence of cell migration alterations within the cardiac OFT. *ex vivo* culture of the neural tube during

earlier developmental stages could also provide insight into the role Yap/Taz have on the preliminary stages of NC migration.

Regarding migration, the ECM contains many components that are necessary for cell migration and motility. ECM composition of the heart varies between different tissues and is commonly associated with mechanical stress, an increasingly considerable regulator of cell behavior important for cardiac physiology [94-98]. It is known that Yap/Taz are highly sensitive to mechanical stress and that the ECM proteoglycan agrin may regulate heart regeneration [99,100]. However, the connection between the Hippo signaling pathway and the ECM during cardiac development, and more specifically within the NC population, has yet to be uncovered and would be important for future work.

Lastly, our phenotypic data has established a model for studying CHD, as the phenotypes observed in our *Yap/Taz* deficient mice resemble phenotypes in human CHD patients. CHD is a detrimental disease that affects thousands of newborns every year and unfortunately contributes greatly to the number of pre-term deaths. The high clinical impact of our determined phenotypes has prompted us to explore the potential contribution of the Hippo signaling components in CHD patients. It will be interesting, in collaboration with a physician-scientist, to investigate if Yap and Taz are found altered in cardiac tissue collected from pediatric patients with CHDs similar to those present in our mouse model. This would strengthen our findings and reveal a possible new lead for treatment discoveries, while simultaneously providing insight into the potential roles Yap and Taz have in other cardiac diseases.

5.3 Conclusions

Here, we report that the Hippo signaling effectors Yap and Taz are necessary for proper NC-derived cardiac development. Conditional combinational deficiencies of *Yap* and *Taz* led to cardiac defects similar to phenotypes present with CHD. Furthermore, our data show that Yap/Taz have the potential to regulate NC migration, while not affecting NC proliferation, smooth muscle differentiation, and apoptosis, at early cardiac developmental time points. Interestingly, we noted that the severity of the defects corresponded with the type of combinational deficiency. This indicates that Yap/Taz likely work in a dose-dependent manner. Furthermore, we note that Yap/Taz display functional redundancy, in that Yap is more dominant over Taz. Our findings provide a better understanding of genetic regulations through the NC for cardiac development and disease onset, which could provide great benefit for clinical research of CHDs in human patients.

Chapter 6: Bibliography

1. Arackal, A.; Alsayouri, K. Histology, Heart. In *StatPearls*; Treasure Island (FL), 2022.
2. Bamalan, O.A.; Soos, M.P. Anatomy, Thorax, Heart Great Vessels. In *StatPearls*; Treasure Island (FL), 2022.
3. Brade, T.; Pane, L.S.; Moretti, A.; Chien, K.R.; Laugwitz, K.L. Embryonic heart progenitors and cardiogenesis. *Cold Spring Harb Perspect Med* **2013**, *3*, a013847, doi:10.1101/cshperspect.a013847.
4. Tan, C.M.J.; Lewandowski, A.J. The Transitional Heart: From Early Embryonic and Fetal Development to Neonatal Life. *Fetal Diagn Ther* **2020**, *47*, 373-386, doi:10.1159/000501906.
5. Gunthel, M.; Barnett, P.; Christoffels, V.M. Development, Proliferation, and Growth of the Mammalian Heart. *Mol Ther* **2018**, *26*, 1599-1609, doi:10.1016/j.ymthe.2018.05.022.
6. Buijtendijk, M.F.J.; Barnett, P.; van den Hoff, M.J.B. Development of the human heart. *Am J Med Genet C Semin Med Genet* **2020**, *184*, 7-22, doi:10.1002/ajmg.c.31778.
7. Kirby, M.L.; Waldo, K.L. Neural crest and cardiovascular patterning. *Circulation research* **1995**, *77*, 211-215, doi:10.1161/01.res.77.2.211.
8. George, R.M.; Maldonado-Velez, G.; Firulli, A.B. The heart of the neural crest: cardiac neural crest cells in development and regeneration. *Development* **2020**, *147*, doi:10.1242/dev.188706.

9. Erhardt, S.; Zheng, M.; Zhao, X.; Le, T.P.; Findley, T.O.; Wang, J. The Cardiac Neural Crest Cells in Heart Development and Congenital Heart Defects. *J Cardiovasc Dev Dis* **2021**, *8*, doi:10.3390/jcdd8080089.

10. Ahlstrom, J.D.; Erickson, C.A. The neural crest epithelial-mesenchymal transition in 4D: a 'tail' of multiple non-obligatory cellular mechanisms. *Development* **2009**, *136*, 1801-1812, doi:10.1242/dev.034785.

11. Acloque, H.; Adams, M.S.; Fishwick, K.; Bronner-Fraser, M.; Nieto, M.A. Epithelial-mesenchymal transitions: the importance of changing cell state in development and disease. *The Journal of clinical investigation* **2009**, *119*, 1438-1449, doi:10.1172/JCI38019.

12. Kobayashi, G.S.; Musso, C.M.; Moreira, D.P.; Pontillo-Guimaraes, G.; Hsia, G.S.P.; Caires-Junior, L.C.; Goulart, E.; Passos-Bueno, M.R. Recapitulation of Neural Crest Specification and EMT via Induction from Neural Plate Border-like Cells. *Stem Cell Reports* **2020**, *15*, 776-788, doi:10.1016/j.stemcr.2020.07.023.

13. Bhatt, S.; Diaz, R.; Trainor, P.A. Signals and switches in Mammalian neural crest cell differentiation. *Cold Spring Harb Perspect Biol* **2013**, *5*, doi:10.1101/cshperspect.a008326.

14. Achilleos, A.; Trainor, P.A. Neural crest stem cells: discovery, properties and potential for therapy. *Cell Res* **2012**, *22*, 288-304, doi:10.1038/cr.2012.11.

15. Hutchins, E.J.; Kunttas, E.; Piacentino, M.L.; Howard, A.G.A.t.; Bronner, M.E.; Uribe, R.A. Migration and diversification of the vagal neural crest. *Developmental biology* **2018**, *444 Suppl 1*, S98-S109, doi:10.1016/j.ydbio.2018.07.004.

16. Kirby, M.L.; Turnage, K.L., 3rd; Hays, B.M. Characterization of conotruncal malformations following ablation of "cardiac" neural crest. *The Anatomical record* **1985**, *213*, 87-93, doi:10.1002/ar.1092130112.

17. Kirby, M.L.; Gale, T.F.; Stewart, D.E. Neural crest cells contribute to normal aorticopulmonary septation. *Science* **1983**, *220*, 1059-1061, doi:10.1126/science.6844926.

18. Ma, P.; Gu, S.; Karunamuni, G.H.; Jenkins, M.W.; Watanabe, M.; Rollins, A.M. Cardiac neural crest ablation results in early endocardial cushion and hemodynamic flow abnormalities. *Am J Physiol Heart Circ Physiol* **2016**, *311*, H1150-H1159, doi:10.1152/ajpheart.00188.2016.

19. Waldo, K.; Zdanowicz, M.; Burch, J.; Kumiski, D.H.; Stadt, H.A.; Godt, R.E.; Creazzo, T.L.; Kirby, M.L. A novel role for cardiac neural crest in heart development. *The Journal of clinical investigation* **1999**, *103*, 1499-1507, doi:10.1172/JCI6501.

20. Waldo, K.; Miyagawa-Tomita, S.; Kumiski, D.; Kirby, M.L. Cardiac neural crest cells provide new insight into septation of the cardiac outflow tract: aortic sac to ventricular septal closure. *Developmental biology* **1998**, *196*, 129-144, doi:10.1006/dbio.1998.8860.

21. Le Lievre, C.S.; Le Douarin, N.M. Mesenchymal derivatives of the neural crest: analysis of chimaeric quail and chick embryos. *Journal of embryology and experimental morphology* **1975**, *34*, 125-154.

22. Jain, R.; Engleka, K.A.; Rentschler, S.L.; Manderfield, L.J.; Li, L.; Yuan, L.; Epstein, J.A. Cardiac neural crest orchestrates remodeling and functional maturation of mouse

semilunar valves. *The Journal of clinical investigation* **2011**, *121*, 422-430, doi:10.1172/JCI44244.

23. Bergwerff, M.; Verberne, M.E.; DeRuiter, M.C.; Poelmann, R.E.; Gittenberger-de Groot, A.C. Neural crest cell contribution to the developing circulatory system: implications for vascular morphology? *Circulation research* **1998**, *82*, 221-231, doi:10.1161/01.res.82.2.221.

24. Waldo, K.L.; Lo, C.W.; Kirby, M.L. Connexin 43 expression reflects neural crest patterns during cardiovascular development. *Developmental biology* **1999**, *208*, 307-323, doi:10.1006/dbio.1999.9219.

25. Sato, M.; Yost, H.J. Cardiac neural crest contributes to cardiomyogenesis in zebrafish. *Developmental biology* **2003**, *257*, 127-139, doi:10.1016/s0012-1606(03)00037-x.

26. Cavanaugh, A.M.; Huang, J.; Chen, J.N. Two developmentally distinct populations of neural crest cells contribute to the zebrafish heart. *Developmental biology* **2015**, *404*, 103-112, doi:10.1016/j.ydbio.2015.06.002.

27. Kolker, S.J.; Tajchman, U.; Weeks, D.L. Confocal imaging of early heart development in Xenopus laevis. *Developmental biology* **2000**, *218*, 64-73, doi:10.1006/dbio.1999.9558.

28. Lee, Y.H.; Saint-Jeannet, J.P. Cardiac neural crest is dispensable for outflow tract septation in Xenopus. *Development* **2011**, *138*, 2025-2034, doi:10.1242/dev.061614.

29. Mohun, T.J.; Leong, L.M.; Weninger, W.J.; Sparrow, D.B. The morphology of heart development in Xenopus laevis. *Developmental biology* **2000**, *218*, 74-88, doi:10.1006/dbio.1999.9559.

30. Zhao, B.; Tumaneng, K.; Guan, K.L. The Hippo pathway in organ size control, tissue regeneration and stem cell self-renewal. *Nat Cell Biol* **2011**, *13*, 877-883, doi:10.1038/ncb2303.

31. Jia, J.; Zhang, W.; Wang, B.; Trinko, R.; Jiang, J. The Drosophila Ste20 family kinase dMST functions as a tumor suppressor by restricting cell proliferation and promoting apoptosis. *Genes Dev* **2003**, *17*, 2514-2519, doi:10.1101/gad.1134003.

32. Halder, G.; Johnson, R.L. Hippo signaling: growth control and beyond. *Development* **2011**, *138*, 9-22, doi:10.1242/dev.045500.

33. Edgar, B.A. From cell structure to transcription: Hippo forges a new path. *Cell* **2006**, *124*, 267-273, doi:10.1016/j.cell.2006.01.005.

34. Wang, J.; Martin, J.F. Hippo Pathway: An Emerging Regulator of Craniofacial and Dental Development. *J Dent Res* **2017**, *96*, 1229-1237, doi:10.1177/0022034517719886.

35. Heallen, T.; Zhang, M.; Wang, J.; Bonilla-Claudio, M.; Klysik, E.; Johnson, R.L.; Martin, J.F. Hippo pathway inhibits Wnt signaling to restrain cardiomyocyte proliferation and heart size. *Science* **2011**, *332*, 458-461, doi:10.1126/science.1199010.

36. Xiao, Y.; Hill, M.C.; Zhang, M.; Martin, T.J.; Morikawa, Y.; Wang, S.; Moise, A.R.; Wythe, J.D.; Martin, J.F. Hippo Signaling Plays an Essential Role in Cell State Transitions during Cardiac Fibroblast Development. *Dev Cell* **2018**, *45*, 153-169 e156, doi:10.1016/j.devcel.2018.03.019.

37. Singh, A.; Ramesh, S.; Cibi, D.M.; Yun, L.S.; Li, J.; Li, L.; Manderfield, L.J.; Olson, E.N.; Epstein, J.A.; Singh, M.K. Hippo Signaling Mediators Yap and Taz Are

Required in the Epicardium for Coronary Vasculature Development. *Cell reports* **2016**, *15*, 1384-1393, doi:10.1016/j.celrep.2016.04.027.

38. Artap, S.; Manderfield, L.J.; Smith, C.L.; Poleshko, A.; Aghajanian, H.; See, K.; Li, L.; Jain, R.; Epstein, J.A. Endocardial Hippo signaling regulates myocardial growth and cardiogenesis. *Developmental biology* **2018**, *440*, 22-30, doi:10.1016/j.ydbio.2018.04.026.

39. Zhou, Q.; Li, L.; Zhao, B.; Guan, K.L. The hippo pathway in heart development, regeneration, and diseases. *Circulation research* **2015**, *116*, 1431-1447, doi:10.1161/CIRCRESAHA.116.303311.

40. Kelly, R.G.; Buckingham, M.E.; Moorman, A.F. Heart fields and cardiac morphogenesis. *Cold Spring Harb Perspect Med* **2014**, *4*, doi:10.1101/cshperspect.a015750.

41. Xin, M.; Kim, Y.; Sutherland, L.B.; Qi, X.; McAnally, J.; Schwartz, R.J.; Richardson, J.A.; Bassel-Duby, R.; Olson, E.N. Regulation of insulin-like growth factor signaling by Yap governs cardiomyocyte proliferation and embryonic heart size. *Sci Signal* **2011**, *4*, ra70, doi:10.1126/scisignal.2002278.

42. von Gise, A.; Lin, Z.; Schlegelmilch, K.; Honor, L.B.; Pan, G.M.; Buck, J.N.; Ma, Q.; Ishiwata, T.; Zhou, B.; Camargo, F.D.; et al. YAP1, the nuclear target of Hippo signaling, stimulates heart growth through cardiomyocyte proliferation but not hypertrophy. *Proceedings of the National Academy of Sciences of the United States of America* **2012**, *109*, 2394-2399, doi:10.1073/pnas.1116136109.

43. Miesfeld, J.B.; Link, B.A. Establishment of transgenic lines to monitor and manipulate Yap/Taz-Tead activity in zebrafish reveals both evolutionarily conserved

and divergent functions of the Hippo pathway. *Mech Dev* **2014**, *133*, 177-188, doi:10.1016/j.mod.2014.02.003.

44. Wang, J.; Xiao, Y.; Hsu, C.W.; Martinez-Traverso, I.M.; Zhang, M.; Bai, Y.; Ishii, M.; Maxson, R.E.; Olson, E.N.; Dickinson, M.E.; et al. Yap and Taz play a crucial role in neural crest-derived craniofacial development. *Development* **2016**, *143*, 504-515, doi:10.1242/dev.126920.

45. Manderfield, L.J.; Aghajanian, H.; Engleka, K.A.; Lim, L.Y.; Liu, F.; Jain, R.; Li, L.; Olson, E.N.; Epstein, J.A. Hippo signaling is required for Notch-dependent smooth muscle differentiation of neural crest. *Development* **2015**, *142*, 2962-2971, doi:10.1242/dev.125807.

46. Manderfield, L.J.; Engleka, K.A.; Aghajanian, H.; Gupta, M.; Yang, S.; Li, L.; Baggs, J.E.; Hogenesch, J.B.; Olson, E.N.; Epstein, J.A. Pax3 and Hippo Signaling Coordinate Melanocyte Gene Expression in Neural Crest. *Cell reports* **2015**, *10*, 841, doi:10.1016/j.celrep.2015.01.041.

47. Lamar, J.M.; Stern, P.; Liu, H.; Schindler, J.W.; Jiang, Z.G.; Hynes, R.O. The Hippo pathway target, YAP, promotes metastasis through its TEAD-interaction domain. *Proceedings of the National Academy of Sciences of the United States of America* **2012**, *109*, E2441-2450, doi:10.1073/pnas.1212021109.

48. Kumar, D.; Nitzan, E.; Kalcheim, C. YAP promotes neural crest emigration through interactions with BMP and Wnt activities. *Cell Commun Signal* **2019**, *17*, 69, doi:10.1186/s12964-019-0383-x.

49. Vega-Lopez, G.A.; Cerrizuela, S.; Tribulo, C.; Aybar, M.J. Neurocristopathies: New insights 150 years after the neural crest discovery. *Developmental biology* **2018**, *444 Suppl 1*, S110-S143, doi:10.1016/j.ydbio.2018.05.013.

50. Zhao, X.; Le, T.P.; Erhardt, S.; Findley, T.O.; Wang, J. Hippo-Yap Pathway Orchestrates Neural Crest Ontogenesis. *Front Cell Dev Biol* **2021**, *9*, 706623, doi:10.3389/fcell.2021.706623.

51. Snider, T.N.; Mishina, Y. Cranial neural crest cell contribution to craniofacial formation, pathology, and future directions in tissue engineering. *Birth Defects Res C Embryo Today* **2014**, *102*, 324-332, doi:10.1002/bdrc.21075.

52. Okuno, H.; Okano, H. Modeling human congenital disorders with neural crest developmental defects using patient-derived induced pluripotent stem cells. *Regen Ther* **2021**, *18*, 275-280, doi:10.1016/j.reth.2021.08.001.

53. Maguire, L.H.; Thomas, A.R.; Goldstein, A.M. Tumors of the neural crest: Common themes in development and cancer. *Dev Dyn* **2015**, *244*, 311-322, doi:10.1002/dvdy.24226.

54. Lee, G.; Studer, L. Modelling familial dysautonomia in human induced pluripotent stem cells. *Philos Trans R Soc Lond B Biol Sci* **2011**, *366*, 2286-2296, doi:10.1098/rstb.2011.0026.

55. Lopes, S.; Guimaraes, I.C.B.; Costa, S.F.O.; Acosta, A.X.; Sandes, K.A.; Mendes, C.M.C. Mortality for Critical Congenital Heart Diseases and Associated Risk Factors in Newborns. A Cohort Study. *Arq Bras Cardiol* **2018**, *111*, 666-673, doi:10.5935/abc.20180175.

56. Wu, W.; He, J.; Shao, X. Incidence and mortality trend of congenital heart disease at the global, regional, and national level, 1990-2017. *Medicine* **2020**, *99*, e20593, doi:10.1097/MD.0000000000020593.

57. van der Linde, D.; Konings, E.E.; Slager, M.A.; Witsenburg, M.; Helbing, W.A.; Takkenberg, J.J.; Roos-Hesselink, J.W. Birth prevalence of congenital heart disease worldwide: a systematic review and meta-analysis. *Journal of the American College of Cardiology* **2011**, *58*, 2241-2247, doi:10.1016/j.jacc.2011.08.025.

58. Lynge, T.H.; Jeppesen, A.G.; Winkel, B.G.; Glinge, C.; Schmidt, M.R.; Sondergaard, L.; Risgaard, B.; Tfelt-Hansen, J. Nationwide Study of Sudden Cardiac Death in People With Congenital Heart Defects Aged 0 to 35 Years. *Circ Arrhythm Electrophysiol* **2018**, *11*, e005757, doi:10.1161/CIRCEP.117.005757.

59. Becker, A.E.; Anderson, R.H. Classification of ventricular septal defects--a matter of precision. *Heart Vessels* **1985**, *1*, 120-121, doi:10.1007/BF02066359.

60. Roguin, N.; Du, Z.D.; Barak, M.; Nasser, N.; Hershkowitz, S.; Milgram, E. High prevalence of muscular ventricular septal defect in neonates. *Journal of the American College of Cardiology* **1995**, *26*, 1545-1548, doi:10.1016/0735-1097(95)00358-4.

61. Craig, R.J.; Selzer, A. Natural history and prognosis of atrial septal defect. *Circulation* **1968**, *37*, 805-815, doi:10.1161/01.cir.37.5.805.

62. Hermes-DeSantis, E.R.; Clyman, R.I. Patent ductus arteriosus: pathophysiology and management. *J Perinatol* **2006**, *26 Suppl 1*, S14-18; discussion S22-13, doi:10.1038/sj.jp.7211465.

63. Benitz, W.E.; Committee on, F.; Newborn, A.A.o.P. Patent Ductus Arteriosus in Preterm Infants. *Pediatrics* **2016**, *137*, doi:10.1542/peds.2015-3730.

64. Obler, D.; Juraszek, A.L.; Smoot, L.B.; Natowicz, M.R. Double outlet right ventricle: aetiologies and associations. *J Med Genet* **2008**, *45*, 481-497, doi:10.1136/jmg.2008.057984.

65. Collett, R.W.; Edwards, J.E. Persistent truncus arteriosus; a classification according to anatomic types. *Surg Clin North Am* **1949**, *29*, 1245-1270, doi:10.1016/s0039-6109(16)32803-1.

66. Hsu, P.; Ma, A.; Wilson, M.; Williams, G.; Curotta, J.; Munns, C.F.; Mehr, S. CHARGE syndrome: a review. *J Paediatr Child Health* **2014**, *50*, 504-511, doi:10.1111/jpc.12497.

67. Bond, A.M.; Bhalala, O.G.; Kessler, J.A. The dynamic role of bone morphogenetic proteins in neural stem cell fate and maturation. *Developmental neurobiology* **2012**, *72*, 1068-1084, doi:10.1002/dneu.22022.

68. Goldstein, A.M.; Brewer, K.C.; Doyle, A.M.; Nagy, N.; Roberts, D.J. BMP signaling is necessary for neural crest cell migration and ganglion formation in the enteric nervous system. *Mech Dev* **2005**, *122*, 821-833, doi:10.1016/j.mod.2005.03.003.

69. Bai, Y.; Wang, J.; Morikawa, Y.; Bonilla-Claudio, M.; Klysik, E.; Martin, J.F. Bmp signaling represses Vegfa to promote outflow tract cushion development. *Development* **2013**, *140*, 3395-3402, doi:10.1242/dev.097360.

70. Wang, J.; Greene, S.B.; Martin, J.F. BMP signaling in congenital heart disease: new developments and future directions. *Birth Defects Res A Clin Mol Teratol* **2011**, *91*, 441-448, doi:10.1002/bdra.20785.

71. Zheng, M.; Erhardt, S.; Ai, D.; Wang, J. Bmp Signaling Regulates Hand1 in a Dose-Dependent Manner during Heart Development. *Int J Mol Sci* **2021**, *22*, doi:10.3390/ijms22189835.

72. Stottmann, R.W.; Choi, M.; Mishina, Y.; Meyers, E.N.; Klingensmith, J. BMP receptor IA is required in mammalian neural crest cells for development of the cardiac outflow tract and ventricular myocardium. *Development* **2004**, *131*, 2205-2218, doi:10.1242/dev.01086.

73. Jia, Q.; McDill, B.W.; Li, S.Z.; Deng, C.; Chang, C.P.; Chen, F. Smad signaling in the neural crest regulates cardiac outflow tract remodeling through cell autonomous and non-cell autonomous effects. *Developmental biology* **2007**, *311*, 172-184, doi:10.1016/j.ydbio.2007.08.044.

74. Cappuccio, G.; Brunetti-Pierri, N.; Clift, P.; Learn, C.; Dykes, J.C.; Mercer, C.L.; Callewaert, B.; Meerschaut, I.; Spinelli, A.M.; Bruno, I.; et al. Expanded cardiovascular phenotype of Myhre syndrome includes tetralogy of Fallot suggesting a role for SMAD4 in human neural crest defects. *Am J Med Genet A* **2022**, *188*, 1384-1395, doi:10.1002/ajmg.a.62645.

75. Firulli, A.B.; McFadden, D.G.; Lin, Q.; Srivastava, D.; Olson, E.N. Heart and extra-embryonic mesodermal defects in mouse embryos lacking the bHLH transcription factor Hand1. *Nat Genet* **1998**, *18*, 266-270, doi:10.1038/ng0398-266.

76. Firulli, A.B. A HANDful of questions: the molecular biology of the heart and neural crest derivatives (HAND)-subclass of basic helix-loop-helix transcription factors. *Gene* **2003**, *312*, 27-40, doi:10.1016/s0378-1119(03)00669-3.

77. Holler, K.L.; Hendershot, T.J.; Troy, S.E.; Vincentz, J.W.; Firulli, A.B.; Howard, M.J. Targeted deletion of Hand2 in cardiac neural crest-derived cells influences cardiac gene expression and outflow tract development. *Developmental biology* **2010**, *341*, 291-304, doi:10.1016/j.ydbio.2010.02.001.

78. Sanchez, J.; Miyake, R.; Cheng, A.; Liu, T.; Iseki, S.; Kume, T. Conditional inactivation of Foxc1 and Foxc2 in neural crest cells leads to cardiac abnormalities. *Genesis* **2020**, *58*, e23364, doi:10.1002/dvg.23364.

79. McElhinney, D.B.; Krantz, I.D.; Bason, L.; Piccoli, D.A.; Emerick, K.M.; Spinner, N.B.; Goldmuntz, E. Analysis of cardiovascular phenotype and genotype-phenotype correlation in individuals with a JAG1 mutation and/or Alagille syndrome. *Circulation* **2002**, *106*, 2567-2574, doi:10.1161/01.cir.0000037221.45902.69.

80. Varadkar, P.; Kraman, M.; Despres, D.; Ma, G.; Lozier, J.; McCright, B. Notch2 is required for the proliferation of cardiac neural crest-derived smooth muscle cells. *Dev Dyn* **2008**, *237*, 1144-1152, doi:10.1002/dvdy.21502.

81. Yan, S.; Thienthanasit, R.; Chen, D.; Engelen, E.; Bruhl, J.; Crossman, D.K.; Kesterson, R.; Wang, Q.; Bouazoune, K.; Jiao, K. CHD7 regulates cardiovascular development through ATP-dependent and -independent activities. *Proceedings of the National Academy of Sciences of the United States of America* **2020**, *117*, 28847-28858, doi:10.1073/pnas.2005222117.

82. Kioussi, C.; Briata, P.; Baek, S.H.; Rose, D.W.; Hamblet, N.S.; Herman, T.; Ohgi, K.A.; Lin, C.; Gleiberman, A.; Wang, J.; et al. Identification of a Wnt/Dvl/beta-Catenin --> Pitx2 pathway mediating cell-type-specific proliferation during development. *Cell* **2002**, *111*, 673-685, doi:10.1016/s0092-8674(02)01084-x.

83. Ganji, H.; Salehi, M.; Sedghi, M.; Abdali, H.; Nouri, N.; Sadri, L.; Hosseinzadeh, M.; Vakili, B.; Lotfi, M. Investigation of TBX1 gene deletion in Iranian children with 22q11.2 deletion syndrome: correlation with conotruncal heart defects. *Heart Asia* **2013**, *5*, 200-202, doi:10.1136/heartasia-2013-010327.

84. Lewis, A.E.; Vasudevan, H.N.; O'Neill, A.K.; Soriano, P.; Bush, J.O. The widely used Wnt1-Cre transgene causes developmental phenotypes by ectopic activation of Wnt signaling. *Developmental biology* **2013**, *379*, 229-234, doi:10.1016/j.ydbio.2013.04.026.

85. Calmont, A.; Ivins, S.; Van Bueren, K.L.; Papangeli, I.; Kyriakopoulou, V.; Andrews, W.D.; Martin, J.F.; Moon, A.M.; Illingworth, E.A.; Basson, M.A.; et al. Tbx1 controls cardiac neural crest cell migration during arch artery development by regulating Gbx2 expression in the pharyngeal ectoderm. *Development* **2009**, *136*, 3173-3183, doi:10.1242/dev.028902.

86. Dinsmore, C.J.; Ke, C.Y.; Soriano, P. The Wnt1-Cre2 transgene is active in the male germline. *Genesis* **2022**, *60*, e23468, doi:10.1002/dvg.23468.

87. Ishii, M.; Arias, A.C.; Liu, L.; Chen, Y.B.; Bronner, M.E.; Maxson, R.E. A stable cranial neural crest cell line from mouse. *Stem Cells Dev* **2012**, *21*, 3069-3080, doi:10.1089/scd.2012.0155.

88. Misra, J.R.; Irvine, K.D. The Hippo Signaling Network and Its Biological Functions. *Annu Rev Genet* **2018**, *52*, 65-87, doi:10.1146/annurev-genet-120417-031621.

89. Yang, D.; Zhang, N.; Li, M.; Hong, T.; Meng, W.; Ouyang, T. The Hippo Signaling Pathway: The Trader of Tumor Microenvironment. *Front Oncol* **2021**, *11*, 772134, doi:10.3389/fonc.2021.772134.

90. Barron, D.A.; Kagey, J.D. The role of the Hippo pathway in human disease and tumorigenesis. *Clin Transl Med* **2014**, *3*, 25, doi:10.1186/2001-1326-3-25.

91. Moya, I.M.; Halder, G. Hippo-YAP/TAZ signalling in organ regeneration and regenerative medicine. *Nat Rev Mol Cell Biol* **2019**, *20*, 211-226, doi:10.1038/s41580-018-0086-y.

92. Wang, Y.; Yu, A.; Yu, F.X. The Hippo pathway in tissue homeostasis and regeneration. *Protein Cell* **2017**, *8*, 349-359, doi:10.1007/s13238-017-0371-0.

93. Zheng, M.; Jacob, J.; Hung, S.H.; Wang, J. The Hippo Pathway in Cardiac Regeneration and Homeostasis: New Perspectives for Cell-Free Therapy in the Injured Heart. *Biomolecules* **2020**, *10*, doi:10.3390/biom10071024.

94. Lockhart, M.; Wirrig, E.; Phelps, A.; Wessels, A. Extracellular matrix and heart development. *Birth Defects Res A Clin Mol Teratol* **2011**, *91*, 535-550, doi:10.1002/bdra.20810.

95. Icardo, J.M.; Colvee, E. Atrioventricular valves of the mouse: III. Collagenous skeleton and myotendinous junction. *The Anatomical record* **1995**, *243*, 367-375, doi:10.1002/ar.1092430311.

96. Pankov, R.; Yamada, K.M. Fibronectin at a glance. *J Cell Sci* **2002**, *115*, 3861-3863, doi:10.1242/jcs.00059.

97. Hurle, J.M.; Kitten, G.T.; Sakai, L.Y.; Volpin, D.; Solursh, M. Elastic extracellular matrix of the embryonic chick heart: an immunohistological study using laser confocal microscopy. *Dev Dyn* **1994**, *200*, 321-332, doi:10.1002/aja.1002000407.

98. Rauch, U.; Schafer, K.H. The extracellular matrix and its role in cell migration and development of the enteric nervous system. *Eur J Pediatr Surg* **2003**, *13*, 158-162, doi:10.1055/s-2003-41265.

99. Dupont, S.; Morsut, L.; Aragona, M.; Enzo, E.; Giulitti, S.; Cordenonsi, M.; Zanconato, F.; Le Digabel, J.; Forcato, M.; Bicciato, S.; et al. Role of YAP/TAZ in mechanotransduction. *Nature* **2011**, *474*, 179-183, doi:10.1038/nature10137.

100. Bassat, E.; Mutlak, Y.E.; Genzelinakh, A.; Shadrin, I.Y.; Baruch Umansky, K.; Yifa, O.; Kain, D.; Rajchman, D.; Leach, J.; Riabov Bassat, D.; et al. The extracellular matrix protein agrin promotes heart regeneration in mice. *Nature* **2017**, *547*, 179-184, doi:10.1038/nature22978.

Vita

Shannon Nicole Erhardt was born in Winfield, Illinois, the daughter of Catherine Ann Erhardt and Gary Klous Erhardt. After completing her work at Wheaton Warrenville South High School, Wheaton, Illinois in 2016, she entered Iowa State University, Ames, Iowa. She received a Bachelor of Science with a major in Genetics in May 2020, and graduate cum laude. In August 2020 she entered the University of Texas MD Anderson Cancer Center UTHealth Graduate School of Biomedical Sciences.

Permanent address: 1 Hermann Park Ct. Apt 848, Houston, Texas, 77018.